

Article

Ultrastructural Remodeling of the Neurovascular Unit in the Female Diabetic db/db Model—Part I: Astrocyte

Melvin R. Hayden ^{1,2,*}, DeAna G. Grant ³, Annayya R. Aroor ^{1,2,4}  and Vincent G. DeMarco ^{1,2,4,5} 

¹ Diabetes and Cardiovascular Center, University of Missouri School of Medicine, Columbia, MO 65212, USA; aroora@health.missouri.edu (A.R.A.); demarcov@missouri.edu (V.G.D.)

² Division of Endocrinology and Metabolism, Department of Medicine, University of Missouri, Columbia, MO 65211, USA

³ Electron Microscopy Core Facility, University of Missouri, Columbia, MO 65211, USA; GrantDe@missouri.edu

⁴ Research Service, Harry S. Truman Memorial Veterans Hospital, Columbia, MO 65201, USA

⁵ Department of Medical Pharmacology and Physiology, University of Missouri, Columbia, MO 65211, USA

* Correspondence: mrh29pete@gmail.com; Tel.: +1-573-346-3019

Received: 4 July 2018; Accepted: 31 July 2018; Published: 7 August 2018



Abstract: Obesity, insulin resistance, and type 2 diabetes mellitus are associated with cognitive impairment, known as diabetic cognopathy. In this study, we tested the hypothesis that neurovascular unit(s) (NVU) within cerebral cortical gray matter regions display abnormal cellular remodeling. The monogenic (*Lepr^{db}*) female diabetic db/db (BKS.CgDock7^m +/+*Lepr^{db}*/J; DBC) mouse model was utilized for this ultrastructural study. Upon sacrifice (at 20 weeks of age), left-brain hemispheres of the DBC and age-matched non-diabetic wild-type control C57BL/KsJ (CKC) mice were immediately immersion-fixed. We found attenuation/loss of endothelial blood–brain barrier tight/adherens junctions and pericytes, thickening of the basement membrane, aberrant mitochondria, and pathological remodeling of protoplasmic astrocytes. Additionally, there were adherent red blood cells and NVU microbleeds (cortical layer III) in DBC mice, which were not observed in CKC animals. While this study represents only a “snapshot in time”, it does allow for cellular remodeling comparisons between DBC and CKC. In this paper, the first of a three-part series, we report the observational ultrastructural remodeling changes of the NVU and its protoplasmic astrocytes in relation to the surrounding neuropil. Having identified multiple abnormal cellular remodeling changes in the DBC as compared to CKC models, we will design future experiments to evaluate various treatment modalities in DBC mice.

Keywords: astrocyte; db/db mouse model; microglia; neuroglia; neurovascular unit; type 2 diabetes

1. Introduction

Type 2 diabetes mellitus (T2DM) is a chronic endocrine-metabolic disorder of glucose metabolism characterized by hyperglycemia, insulin resistance or relative lack of insulin and impaired cognition. Type 2 diabetes mellitus is one of the fastest growing public health problems and diseases globally with aging of the global population playing an important role, including the global post-World War II baby boom generation [1]. Concurrently, the prevalence of the age-related neurodegenerative diseases, such as Alzheimer’s disease (AD), vascular dementia, and Parkinson’s disease (PD), are also increasing [2,3]. Importantly, AD may now be considered a mixed dementia consisting of both neurovascular dysfunction (macrovascular and microvascular disease) and neurodegeneration [4–8].

Type 2 diabetes mellitus and AD are each projected to undergo a marked increase in incidence over the coming decades and may indeed be synergistic [9].

Epidemiologic studies identified T2DM as an independent risk factor for multiple affected target organs, which include neuropathy, retinopathy, nephropathy, cardiomyopathy, and the age-related neurodegenerative diseases, such as diabetic cognopathy and AD [10–13]. Neurovascular unit (NVU) and microvascular small vessel disease remodeling are known to be associated with T2DM and age-related neurodegeneration, which are a growing concern. Thus, we elected to study the ultrastructural remodeling changes of the NVU in the mid-cortical gray matter regions of the obese, insulin-resistant, and diabetic female db/db mice models (DBC), and compared them to the lean, non-diabetic, and aged-matched control models (CKC).

The NVU is a complex functional and anatomical structure comprised of endothelial cells (ECs), pericytes (Pcs), astrocytes (ACs), microglia cells (MGCs), and neurons [14]. The luminal ECs contain the blood–brain barrier (BBB), which is formed by tight junction proteins (TJs; claudin, occludin, and junctional adherens molecule proteins) and adherens junction proteins (AJs; vascular endothelial (VE) cadherins), intertwined to form very electron-dense lines at the overlapping junctional inter-endothelial spaces. The TJ/AJ are anchored by adjacent EC zonula occludens-1 (ZO-1) proteins that bind to EC cytoskeleton proteins, which have a highly selective BBB and a high transendothelial electrical resistance, providing a permeability barrier to hydrophilic molecules and large proteins [5,6,8].

The next component of the NVU (proceeding from the luminal EC), is the EC basal lamina or basement membrane (BM), which splits to encase the Pc, which creates an inner and outer BM of the latter. Pericytes provide the mural structural support of the endothelial capillary and NVU. Importantly, pericytes are known to be contractile cells; however, they allow for the dilatation and relaxation of the capillary, when regional neurons are activated, and of signal pericytes via connecting astrocytes [4–8,13–15].

Astrocytes tightly adhere to the BM of both the EC and Pc via its end-feet basal lamina. Astrocytes are responsible for integrating the vascular mural cells (endothelial cells and pericytes) of the NVU to nearby regional neurons [16]. Astrocytes allow for NVU coupling, which is fundamental for the regulation of regional capillary cerebral blood flow (CBF) by both astrocyte and neuron-derived chemical messengers that provide for functional hyperemia; this link is known as neurovascular coupling [14,16,17]. Astrocytes are surrounded by the neuropil, which, in gray matter, is comprised primarily of dendritic synapses and unmyelinated neurons—interneurons with traversing myelinated neurons and an extracellular matrix (ECM) between these cellular structures (Figure 1; Table 1).

We hypothesized that NVU remodeling in the diabetic DBC models is associated with an attenuation and/or loss of endothelial cell BBB TJ/AJ and pericytes similar to our previous findings in the streptozotocin-induced type 1 diabetes mellitus (T1DM) mouse models [18]. Also, we posited that MGCs might undergo a reactive-activation (M1-type polarization) similar to previous observations in the diet-induced obesity and insulin-resistant Western mouse models with intermittent glucose elevation and impaired glucose tolerance [13]. However, in the DBC we observed additional marked abnormal remodeling in the surrounding neuroglial components including astrocytes, microglia, oligodendrocytes, and myelin in addition to our previous findings in type 1 diabetic models and diet-induced obese Western models. The multiple aberrant cellular phenotypes may be associated with increased vulnerability to other age-related diseases such as AD and (PD) in an aging population, which are known to have an increased risk due to T2DM [13,19]. The multicellular ultrastructure morphologic remodeling observed in this study allowed us to become acutely aware that a single cellular structure does not become abnormally remodeled without affecting the structure, and ultimately, the function of other cells in the mid-cortical gray matter of the DBC models. Furthermore, these observations support the notion that no one cell is an island unto itself, and that single maladaptive cell type and dysfunctional remodeling could have a direct or indirect effect on other cells in the same regions as highlighted by the NVU multicellular remodeling in the DBC [20].

Table 1. Identifying characteristics of cells that form the neurovascular unit by transmission electron microscopy.

Mural Cells	
Endothelial cell(s) (EC)	Line the entire vascular system (macrovascular and microvascular) in a mononuclear layer.
	The ECs are the first cell one encounters from the vascular lumen as one proceeds from the luminal surface to the outermost abluminal regions of the neurovascular unit (NVU).
	Endothelial cells have an elusive glycocalyx on their luminal cytoplasm; however, this structure is usually eliminated by dehydration in the preparation for microscopy and staining.
	The ECs have an intermediate electron-dense cytoplasm and are thin except where one encounters a larger and greater electron-dense nucleus.
	Neurovascular ECs have very few to no pinocytotic vesicles as compared to peripheral capillary ECs with an increase in EC mitochondria. Next one encounters the ECs hyaline basement membrane (BM) with a less electron density.
	The ECs cytoplasm and nuclei are elongated and their terminating cytoplasm ends most commonly with overlapping junctions creating a paracellular-inter-endothelial space that is lined by very electron-dense protein staining of tight and adherens junctions that form the brain's specific blood-brain barrier (Figure 1).
Pericyte(s) (Pc)	Are the next abluminal encountered cell in the NVU capillary. Pericytes are embedded within the shared BM synthesized by both the ECs and Pcs. The Pcs wrap around (peri-) the ECs of the NVU capillary and those transitioning to very small arterioles with an internal elastic lamina.
	Similar to the ECs, Pcs have an electron-dense cytoplasm with elongated cytoplasmic processes and nuclei and contain prominent electron-dense lysosomes and mitochondria. Importantly, Pcs are known to be contractile cells that allow for NVU capillary contraction/relaxation to permit relaxation in regions of highly active neurons, which allow for increased regional cerebral blood flow (CBF) and neurovascular coupling (NVC) with intact astrocytes.
	In cross section one sometimes can only identify Pc foot processes (Pcfp) with their encasing inner and outer BMs, whereas in longitudinal sections one can better identify their elongated character (Figure 1)
Glial Cells	
Astrocyte cell(s) (AC)	Are the largest cell of the NVU, which assume a more cuboidal morphology in contrast to ECs and Pcs. The AC are also considered to be the brains connecting cell to regional neurons and form a clear zone, halo or corona around the Pcs and ECs.
	Characteristically, they are the most electron-lucent cell of the NVU and brain cells and one often observes scattered electron-dense line's, which represent their endoplasmic reticulum proteins.
	The ACs electron-dense thinned plasma membranes tightly adhere or abut the outer BMs of the ECs and Pcs. The AC completes the third key cell of the neurovascular unit; however, the microglia are also an important part and in both the grey matter and especially the white matter oligodendrocytes become a highly important part of the NVU as well (Figure 1).
Microglia cells (MGC)	Are the smallest of the glia cells and their cytoplasm is the most electron-dense of the NVU and the brain.
	In their non-activated phenotypic state, they have elongated cytoplasmic process in ramified form. They have an extensive endoplasmic reticulum, Golgi body system and contain multiple mitochondria. Their cytoplasmic processes are known to be capable of extending and contracting. They have a unique morphology of their nuclei with an outer stippled chromatin at its neurolemma and a more stippled diffuse chromatin electron dense appearance of the central nuclei (Figure 1).
Oligodendrocyte cell(s) (OL)	As suggested by their name Oligo-, these cells are intermediate in size and their thinned cytoplasm also have an intermediate electron density that is helpful when comparing to AC and MGCs. They also may occur in groups or nests and are more often found in the deeper white matter regions of the brain
Neurons, Interneurons and the Neuropil	
Neurons (N)-interneurons	May be myelinated or unmyelinated.
	Neurons have electron-lucent cytoplasmic axons with a greater electron dense and orderly layered network of neurofilaments and contain the usual cytoplasmic organelles. Neurons are also known to have and axon hillock and very long cytoplasmic axon extensions, which connect to other neurons via their dendritic synapses.
	Sometimes, neurons and especially interneurons can be noted to be closely interacting and in close proximity to the EC, Pc and astrocytes of the NVU.
	Neuronal cytoplasmic axons are also electron-lucent; however, their more electron-dense neurofilaments are layered in an orderly fashion in contrast to the electron densities of the AC, which are randomly scattered throughout the cytoplasm
Neuropil-neuropile	Is an all-inclusive term and appears to form the background tissue along with a very thinned extracellular matrix-interstitium within the cortical grey matter, which includes the vast number of dendritic synapses, neurons (myelinated/unmyelinated axons) passing through the neuropil along with other glial cells and processes (Figure 1).
	The EC, Pc, AC, MGC, oligodendrocytes and neurons-interneurons are the six major cell types that are present within a vast neuropile responsible for forming the NVU within the cortical grey matter

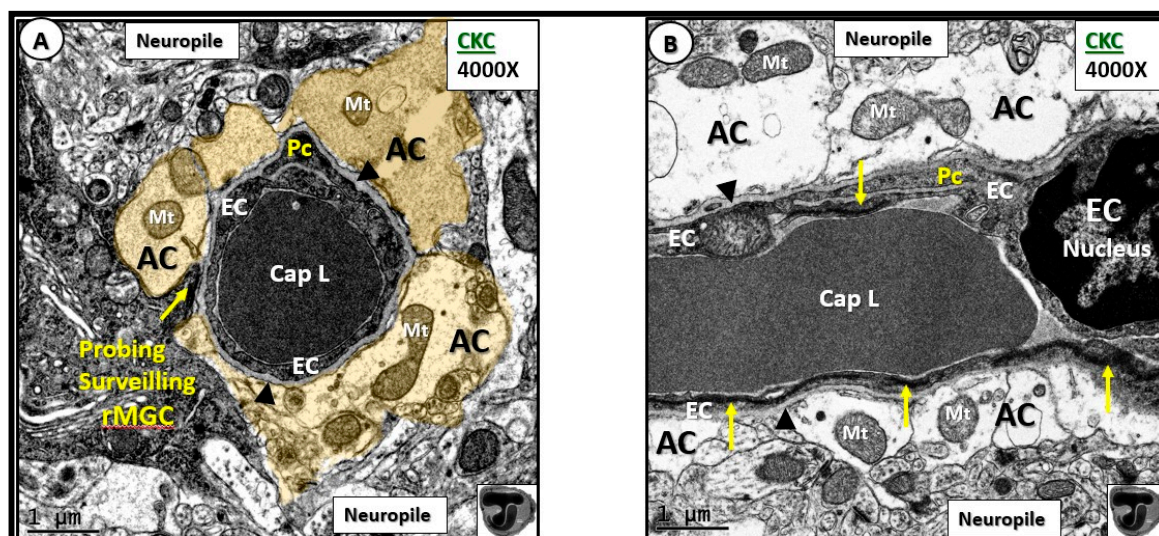


Figure 1. Normal neurovascular unit (NVU) morphology in control wild-type non-diabetic models (C57BL/KsJ; CKC). Panels (A) (cross-section) and (B) (longitudinal section) illustrate the normal cellular ultrastructure of the NVU. Panel (A) depicts an electron-dense ramified microglia cell (rMGC) surveilling the NVU (arrow). The NVU capillary consists of an endothelial cell (EC) encircling a capillary lumen (Cap L) whose basement membrane (BM) splits (arrowheads) to encompass the pericyte (Pc) foot process. Note how the pseudo-colored golden astrocyte (AC) end-feet encompass and tightly abut the capillary EC and Pc BMs. Note that the AC clear zone in panel (A) was pseudo-colored golden to emphasize its importance in the NVU, while it exists as a clear-zone with a reduced electron-dense cytoplasm as compared to other cells within the brain, and represents not only a golden halo, but also a clear zone or corona of ACs surrounding the EC and Pc cells of the NVU (panel (B)). Panel (B) illustrates the electron-lucency of the AC clear zone halo or corona that tightly abuts and encircles the NVU EC and Pc BMs. Note the EC nucleus (far right side) and the highly electron-dense tight junctions/adherens junctions (TJ/AJ) complex that are not readily visible in panel (A) (arrows). Also, note that the mitochondria (Mt) have an electron-dense Mt matrix and that cristae may be noted even at this magnification. Note that the NVU is encompassed by the outermost abluminal neuropil (neuropil). In the bottom right-hand corner, note the logo of red blood cells within a capillary NVU that are in the shape of the letter T overlying the letter J, which are used to abbreviate tight junction(s). Magnification $\times 4000$; scale bar = 1 μm .

2. Methods

2.1. Animal Studies

All animal studies were approved by the Institutional Animal Care and Use Committees at the Harry S Truman Memorial Veterans' Hospital and University of Missouri, Columbia, MO, USA (No. 190), and conformed to the Guide for the Care and Use of Laboratory Animals published by the National Institutes of Health (NIH). Eight-week-old female db/db (BKS.Cg-Dock7^m+/⁺Lepr^{db}/J; DBC) and wild-type control (C57BLKS/J; CKC) mice were purchased from the Jackson Laboratory (Ann Harbor, MI, USA) and were housed under standard laboratory conditions where room temperature was 21–22 °C, and light and dark cycles were 12 h each. Two cohorts of mice were used: lean non-diabetic controls (CKC, $n = 3$), and obese, insulin-resistant, diabetic db/db (DBC, $n = 3$), which were sacrificed for study at 20 weeks of age. The female model was initially chosen because females have greater impairments in diastolic relaxation and increased aortic stiffness, and may predict future cardiovascular disease events [21]. Furthermore, the female gender is positively associated with dementia/AD risk as compared to men (especially in older age groups) [22].

2.2. Tissue Collection and Preparation for Transmission Electron Microscopy

The left hemisphere was collected immediately upon sacrifice in CKC and DBC models and immediately placed in standard transmission electronic microscopy (TEM) fixative of 2% paraformaldehyde and 2% glutaraldehyde in 100 mM sodium cacodylate buffer (pH = 7.35) for immersion fixation. Approximately 1 mm sections from the mid-cortical gray matter tissue (Figure 2) were then rinsed with 100 mM sodium cacodylate buffer (pH 7.35) containing 130 mM sucrose. Secondary fixation was performed using 1% osmium tetroxide (Ted Pella, Inc., Redding, CA, USA) in cacodylate buffer using a Pelco Biowave (Ted Pella) operated at 100 W for 1 min. Specimens were next incubated at 4 °C for 1 h, then rinsed with cacodylate buffer, and further rinsed with distilled water. En bloc staining was performed using 1% aqueous uranyl acetate and incubated at 4 °C overnight, then rinsed with distilled water. Using the Pelco Biowave, a graded dehydration series (e.g., 100 W for 40 s) was performed using ethanol, transitioned into acetone, and dehydrated tissues were then infiltrated with Epon resin (250 W for 3 min) and polymerized at 60 °C overnight. Ultrathin sections were cut to a thickness of 85 nm using an ultramicrotome (Ultracut UCT, Leica Microsystems, Wetzlar, Germany) and stained using Sato's triple lead solution stain and 5% aqueous uranyl acetate. Multiple images were acquired for study at various magnifications with a JOEL 1400-EX TEM JEOL (JEOL, Peabody, MA, USA) at 80 kV on a Gatan Ultrascan 1000 CCD (Gatan, Inc., Pleasanton, CA, USA).

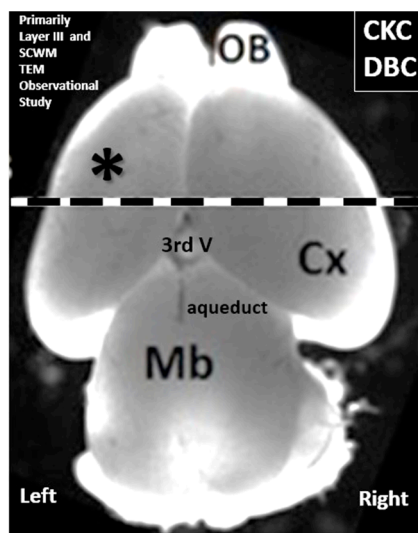


Figure 2. Brain specimens for transmission electron microscopy studies. The left hemisphere was utilized for this study. Cortical gray matter tissue specimens were obtained just cephalad to the mid-cortex dashed line (asterisk). Cx—cerebral cortex; Mb—midbrain; OB—olfactory bulb. TEM—transmission electronic microscopy; V—ventricle; DBC—db/db mice models; SCWM—subcortical with matter.

In regards to utilizing immersion fixation rather than perfusion fixation, the following explanation is in order: in a previous paper, we utilized immersion fixation as a rapid collection and immersion-fixation process of the cortical gray matter study [13]. Since we were interested to provide the same collection and fixation procedures in order to make direct comparisons if necessary, we felt that this collection and fixation method was better suited for our collection team because our previous ultrastructural images appeared to have good penetration of fixative with good fixation for image collection. We are aware and know that perfusion fixation is the preferred method of fixation, and that the immersion fixation is not the most suitable fixation for larger pieces of tissue such as whole brain or the left hemibrain, as in our studies; however, the outermost cortical regions of the brain (layers I–VI and deeper white-matter transitional regions) appear to have fixed nicely via immersion fixation, as can be viewed by our cortical sections in this and our previous paper [13] with distinct ultrastructural morphology. Therefore, because our lab collection team and preparations team previously and

successfully supplied previous immersion-fixed specimens with good results, including cellular outline of membranes, cytoplasmic detail of organelles, nuclear detail, and intra-capillary erythrocyte, as well as white-blood-cell morphologic integrity appearance and overall ultrastructure morphology, and overall staining, we decided that this animal model (db/db diabetic female model) allowed us to utilize the rapid immersion fixation as a method of collecting, fixing, and subsequently studying the ultrastructure (fine structure within the cortical gray matter of the present study). Of interest, these same models were being evaluated using light microscopy, immunohistochemistry, and ultrastructure of other organs, which included the myocardium, aorta, and kidney in forthcoming papers to be published in the near future.

3. Results

In regards to the representation of the image data and images shared in this paper, the following factors are important for understanding our image data: three models per group were studied by TEM ($n = 3$ in control CKC models, and $n = 3$ in db/db DBC models). The sections for study (regions of interest) were selected based on the presence of NVU capillaries, which we were able to identify readily in the cortical layer III of the cortical gray matter. Cortical gray matter layer III is identifiable due to the large number of pyramidal neuronal nuclei. A total of 60 NVU capillaries were eventually studied for all models (10 from each model providing 30 NVU capillaries from CKC, and 30 NVU capillaries from DBC models). The marked remodeling changes observed in the diabetic DBC NVUs and their immediate surrounding regions were immediately noted, and therefore, representative comparison images were primarily chosen at varying magnifications for this paper to better illustrate and understand the marked maladaptive ultrastructure remodeling in the obese, diabetic db/db DBC models as compared to the non-obese non-diabetic CKC models. Therefore, the marked ultrastructural remodeling changes that were observed in the DBC were compared to the CKC. The maladaptive NVU capillaries, which included the attenuation and/or loss of endothelial tight and adherens junctions, thickening of basement membranes, attenuation and/or loss of pericytes, and astrocyte detachment or retraction were approximately 80% of the DBC (24 NVU capillaries with maladaptive remodeling versus a total of 30 NVU capillaries) when compared to no abnormalities (0 of 30 NVU capillaries) in CKC models.

3.1. Endothelial Cell Remodeling of the Neurovascular Unit

Because the BBB is formed primarily by the endothelial cells of the NVU, it seems appropriate to begin with EC remodeling and proceed from the luminal to the abluminal regions (inside-out approach). For reference, the normal ultrastructure morphology of the control model (CKC) NVU is shown in Figure 1.

In obese, diabetic DBCs, we observed an abnormal remodeling of the ECs, which consisted of an attenuation and/or loss of BBB EC TJ/AJ when compared to non-diabetic, non-obese control models (CKC; Figure 3). This attenuated, interrupted, and discontinuous TJ/AJ (Figure 3C), as well as the loss of electron-dense TJ/AJ (Figure 3B,D), may contribute to an increase in the permeability of the blood–brain barrier, as well as NVU uncoupling in the cortex and hippocampus [4,5,7]. Incidentally, when the EC NVU is abnormally remodeled and damaged (especially by oxidative stress due to glucotoxicity and loss of BBB TJ/AJ; Figure 3C), the once-probing surveilling ramified microglial cells (that are operative in control CKC models; Figure 1A) undergo a phenotypic remodeling to a more reactive-activated microglia phenotype as a result of danger and damage signals from the NVU. These reactive-activated microglial cells begin to encircle and invade the NVU (Figure 3C) and may be associated not only with the attenuation and/or loss of EC TJ/AJ, but also with the detachment and retraction of astrocytes to the NVU.

We also observed the NVU basement membrane to be thickened and associated with endothelial cell cytoplasmic thinning, vesicles/vacuoles (ranging in size from approximately 50–200 nm), aberrant mitochondria (aMt), and reactive-activated microglial cells (aMGCs; Figures 3C, 4, and 5). Endothelial cells are primarily responsible for the formation of the NVU basement membrane. The basement membrane is composed of collagen IV, fibrinogen, laminin, nidogen, and heparin sulfate proteoglycans (agrin and perlecan) [23,24]. The basement membrane is important for microvascular development, stability, NVU barrier integrity, and encasement of the pericyte (contributing to BM synthesis and maintenance) and provides the surface for the attachment of astrocyte end-feet. The excessive accumulation and thickening of the basement membrane in some images (Figure 5) were somewhat reminiscent of the thickened mesangial matrix expansion found in renal glomerular diabetic models and humans.

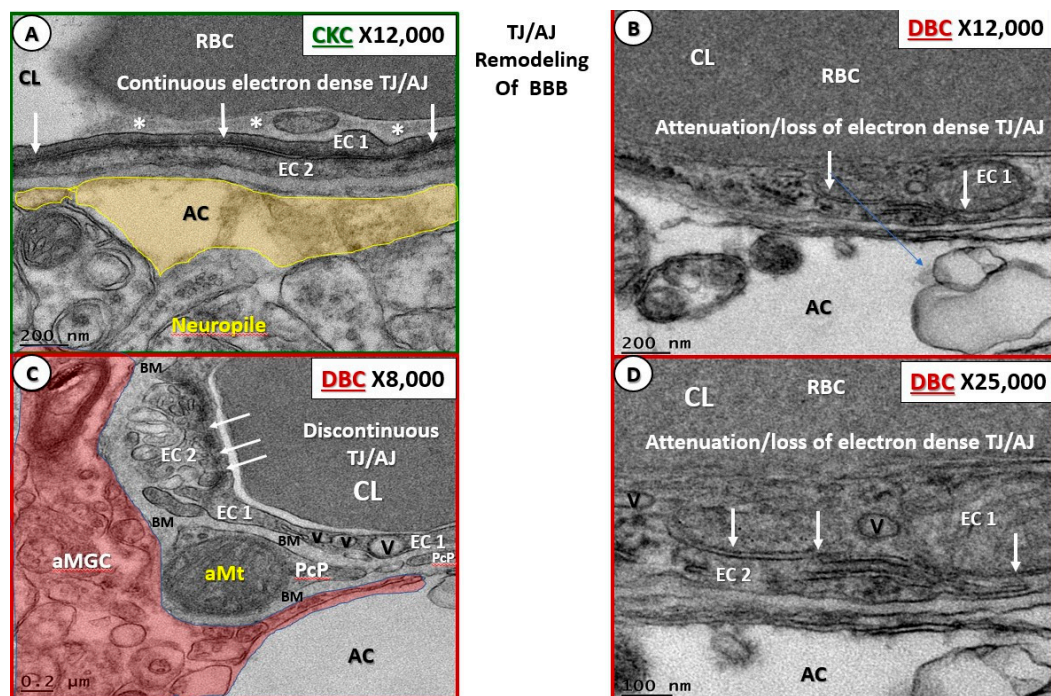


Figure 3. Attenuation and/or loss of tight junctions/adherens junctions (TJ/AJ) in diabetic db/db mice (DBC) models. Panel (A) illustrates the normal appearance of the highly electron-dense proteinaceous endothelial cell (EC) tight junction/adherens junction (TJ/AJ) formed between overlapping ECs. EC-1 overlaps EC-2 in the non-diabetic control models (C57BLKS/J; CKC) to form the paracellular blood–brain barrier (BBB; arrows). This image also depicts the elusive endothelial glycocalyx remnants (asterisks) that form the initial EC barrier of the neurovascular unit (not studied in this experiment). Panel (B) depicts the loss/attenuation of the highly electron-dense proteinaceous TJ/AJ joining the two overlapping EC layers (arrows) in the diabetic DBC models. Magnification $\times 12,000$; scale bar = 200 nm in panels (A,B). Panel (C) illustrates the attenuated, discontinuous, and interrupted morphology of the EC TJ/AJ (arrows) in the obese, diabetic DBC models. Note the pseudo-colored red reactive-activated microglial cell (aMGC) and an abbreviated pericyte process (PcP), which contains an aberrant swollen and smudged mitochondria (aMt). Also, note vacuole (V) and vesicles (v) within the EC cytoplasm of EC 1. Magnification $\times 8000$; scale bar = 0.2 μm . Panel (D) (higher magnification of panel (B)) demonstrates with greater clarity the definite loss of the TJ/AJ electron density depicted in panel (B) as compared to the CKC models in Figures 1B and 3A. Magnification $\times 25,000$; scale bar = 100 nm. AC—astrocyte (pseudo-colored golden panel (A)); CL—capillary lumen; RBC—red blood cell.

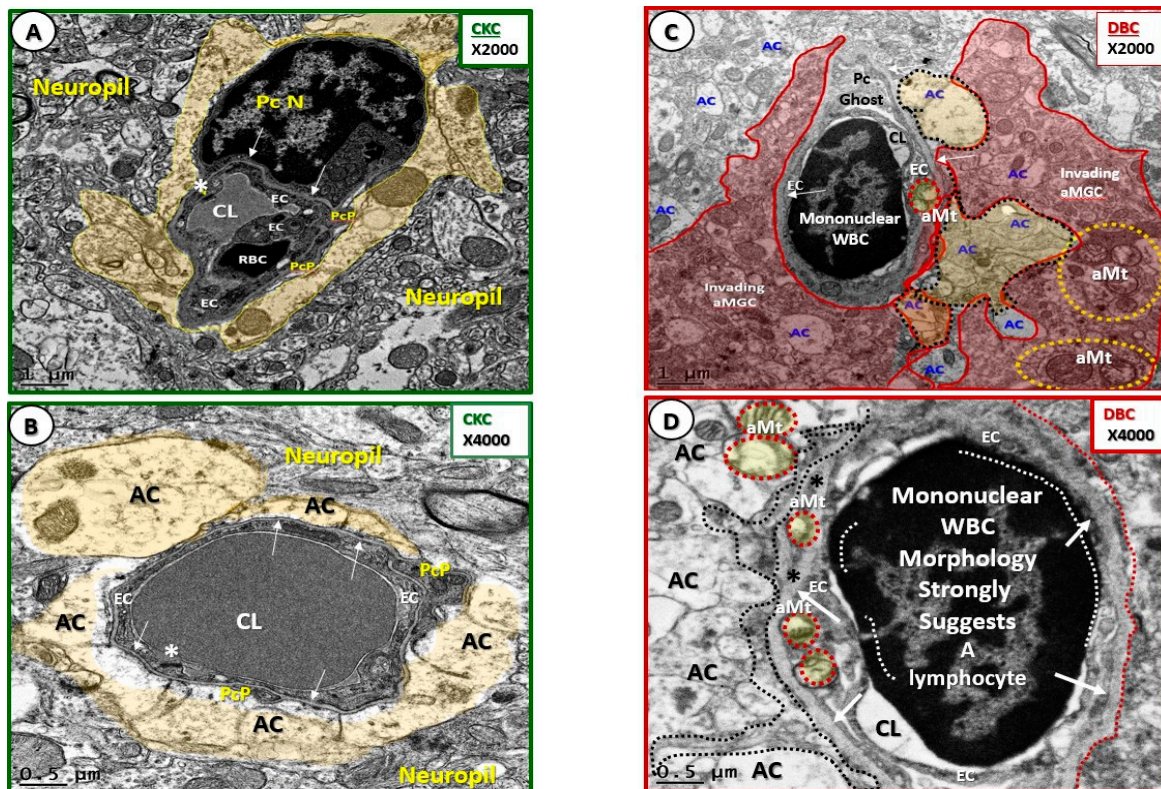


Figure 4. Basement membrane thickening in DBC as compared to control (CKC) models. One can readily observe the thickened ($\geq 200\text{-nm}$ BMs; arrows) in DBC (panels (C,D)) as compared to the normal ($\leq 80\text{-nm}$ BMs (in panels (A,B)) with same magnifications in (A,C) and (B,D)). Magnification $\times 2000$; bar = $1\ \mu\text{m}$ (panel (A)), and magnification $\times 4000$; bar = $0.5\ \mu\text{m}$ (panel (B))). Panel (C) depicts a pericyte ghost smudged region superiorly and an invading reactive-activated microglial cell (pseudo-colored red). Note only the two-remaining intact ACs pseudo-colored golden on the right-hand side of the NVU. Magnification $\times 2000$; bar = $1\ \mu\text{m}$. Panels (C,D) also depict an adherent luminal inflammatory mononuclear cell (dashed white lines in panel (D) = sites of adherence) to the EC. The size and morphology of this mononuclear suggest a lymphocyte. Also note the EC and AC aMt (pseudo-colored yellow with encompassing red dashed lines) and thinning of the EC cytoplasm, especially noted in panel (D) as compared to panel (B). Specifically, in panel (D), one notes an aMGC cytoplasmic process (black-dashed lines) to the left side of this abnormally inflamed NVU, which also illustrates the detachment of the AC from the NVU BM. These combined maladaptive remodeling changes strongly suggest a morphologically activated-dysfunctional endothelium. Magnification $\times 2000$; bar = $1\ \mu\text{m}$ (panel (C)), and magnification $\times 4000$; bar = $0.5\ \mu\text{m}$ (panel (D)). Asterisks—tight junctions/adherens junctions (panels (A,B)); PcN—pericyte nucleus.

3.2. Remodeling of Pericytes and Pericyte Foot Processes

Pericytes are essential for proper formation of the NVU and EC BBB TJ/AJ in utero, as well as for NVU maturation and maintenance during adulthood. As previously mentioned, the basement membrane splits to encompass pericytes and their processes to create an inner and outer BM of pericytes in the NVU (Figures 6 and 7). The brain, including the retina, has the highest coverage of vascular endothelial cells by pericytes, which is essential for regulation of BBB permeability [13]. Pericytes not only contribute to EC BBB TJ/AJ function, but also contribute to basement membrane formation and maintenance [13,15]. Pericytes and endothelial cells share a common basement membrane secured by N-cadherins, fibronectin, connexins, and various integrins-(13, 15, 25). Additionally, pericytes induce the synthesis of occludin and claudin in the endothelial cell TJ/AJ complex through the release of angiopoietin-1 [13]. Endothelial cells also signal to pericytes by synthesizing and secreting

platelet-derived growth factor β (PDGF- β) to activate the Pc-specific receptor (PDGFR- β), which is important for Pc proliferation, migration, and recruitment of Pc to the endothelium [13,25] (Figures 6 and 7).

Key findings in pericyte remodeling included attenuation and/or loss of pericytes and the retraction or loss of pericyte foot processes, in addition to having aberrant Mt within the cytoplasm and the retraction of pericyte nuclei and of pericyte cytoplasmic processes (Figure 7).

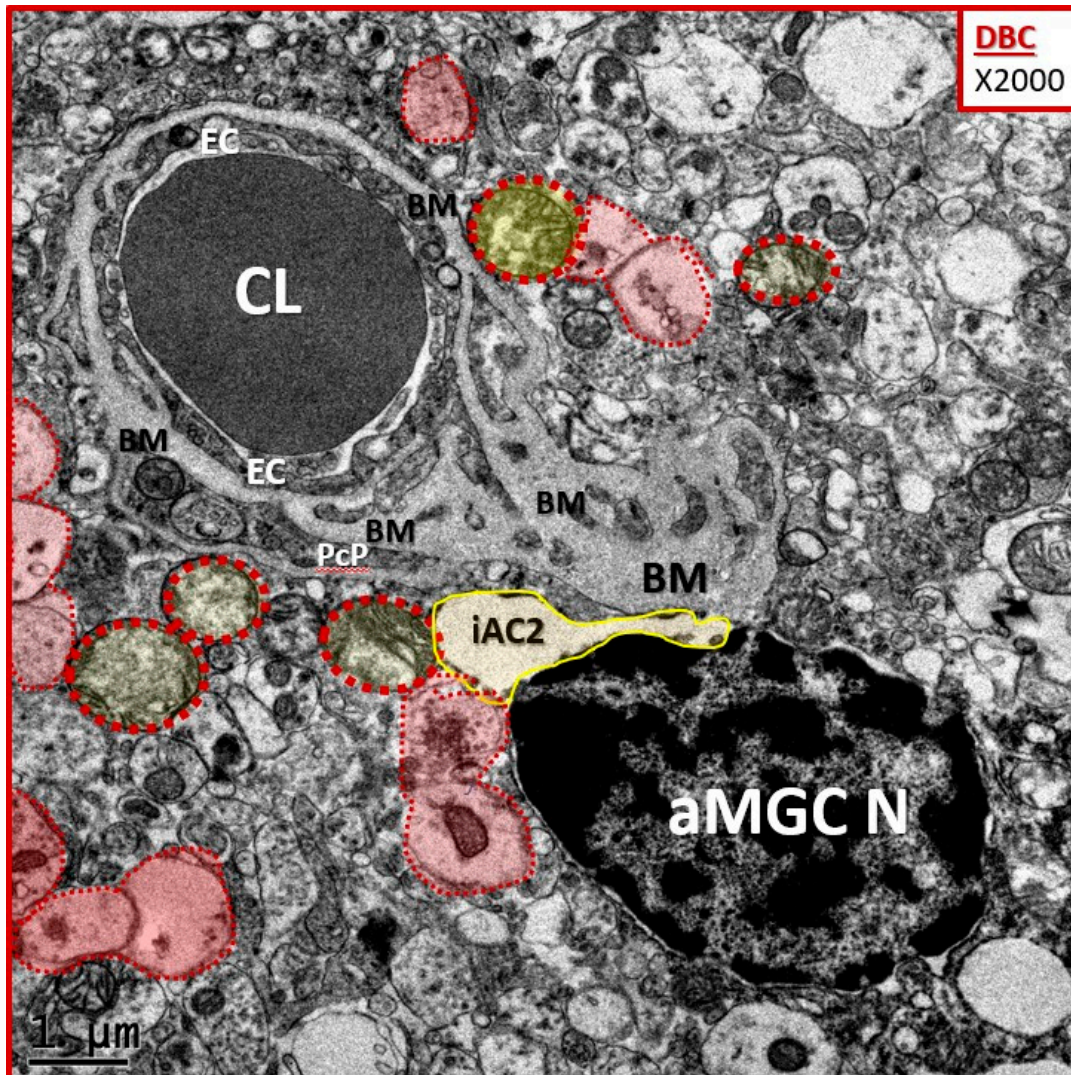


Figure 5. Excessive basement membrane thickening in some DBC models. This image depicts excessive and abundant BM thickening in the NVU of a DBC model. Note that only one intact astrocyte (iAC2) remains in this image (pseudo-colored golden), while the remainder of the ACs are detached and retracted (pseudo-colored red) from the NVU. Note the aMt (pseudo-colored yellow with encapsulating red dashed lines) that are swollen with loss of the electron-dense Mt matrix and loss of cristae. It is important to note the absence of the endothelial cell blood–brain barrier tight and adherent junction complex and pericytes in this image. Importantly, note the detached and retracted astrocytes (pseudo-colored pink with red-dashed outlines). aMGC N—reactive-activated microglial cell nucleus.

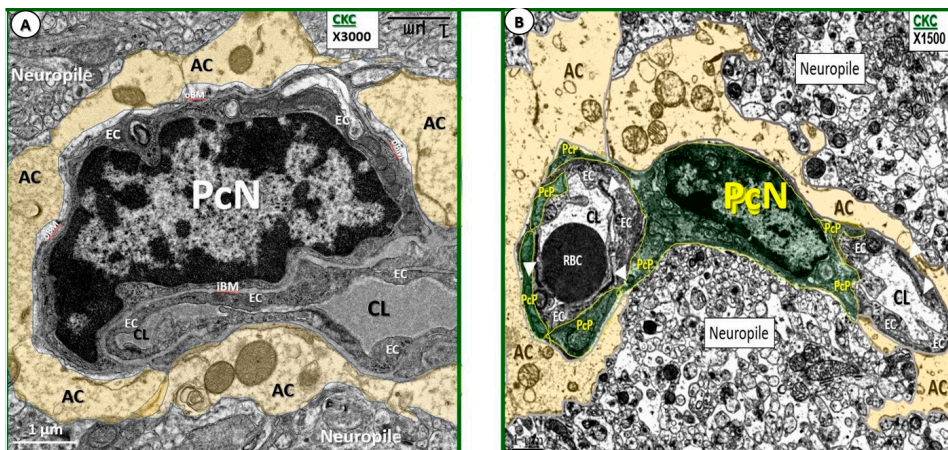


Figure 6. Normal pericyte ultrastructure morphology. Panels (A,B) reflect the normal morphology of the Pc in relation to the NVU in control non-diabetic CKC models. While each of these images contains the soma of a Pc with a PcN), Pcs (pseudo-colored green in panel (B)) are most often observed as PcP, and they are also defined by an inner (iBM) and outer basement membrane (oBM). The Pc and PcP BMs are abutted by the AC's (pseudo-colored gold) basal lamina. While panel (A) demonstrates a single Pc in close relation to the capillary EC of the NVU, one may also observe that Pcs may provide connectivity to two adjacent NVUs as in panel (B). Panel (B) illustrates prominent tight and adherens junctions (TJ/AJ; arrowheads). Also, one will note that in some NVUs, the neuropil may come into direct contact with the outer BM of Pcs. Magnification $\times 3000$; bar = 1 μm (Panel (A)). Magnification $\times 1500$; bar = 1 μm (panel (B)).

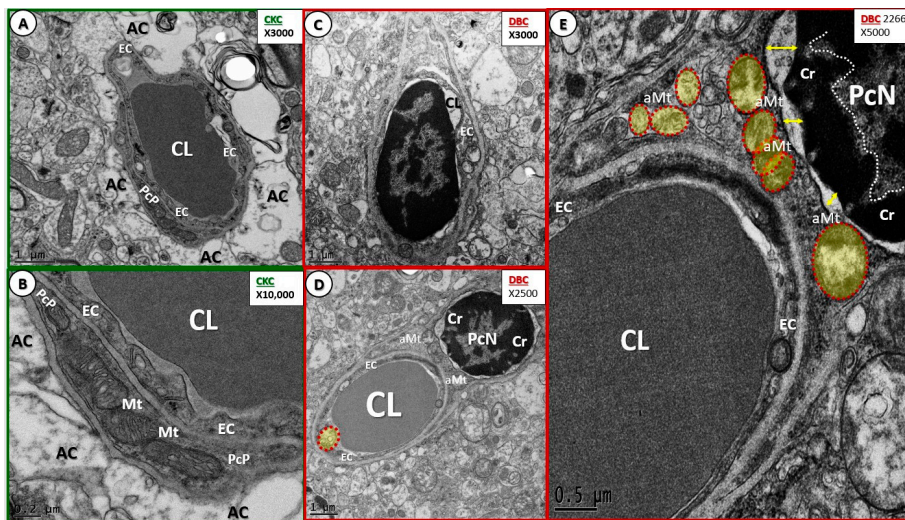


Figure 7. Remodeling of pericytes in diabetic (DBC) models. Panels (A,B) illustrate NVU with normal appearing Pc and PcP. Panels (C-E) demonstrate some of the abnormal Pc remodeling changes that are observed in the diabetic DBC. Panel (C) illustrates the complete loss of PcP in an inflamed abnormally remodeled NVU. Panel (D) depicts an abnormal PcN that is retracted from its nuclear membrane at low magnification to illustrate the NVU surroundings in the neuropil. Also, one will note swollen aMt (pseudo-colored yellow with red dashed-line). Panel E depicts aMt that are pseudo-colored yellow encapsulated by red dashed lines with abnormal swelling, as well as the loss of Mt matrix electron density and the loss of Mt cristae within the cytoplasm of the Pc. This image also depicts the retraction of the PcN from its nuclear membrane (double arrows), and excessive PcN chromatin (Cr) condensation, strongly suggesting Pc dysfunction and degeneration, and may be in the process of eventual loss in DBC. Panels (A,C): magnification $\times 3000$; bar = 1 μm . Panel (B): magnification $\times 10,000$; bar = 0.02 μm . Panel (D): magnification $\times 2500$; bar = 1 μm . Panel (E): magnification $\times 5000$; bar = 0.5 μm .

3.3. Protoplasmic Astrocyte Remodeling in Cortical Gray Matter Diabetic DBC Models

Protoplasmic astrocytes have numerous homeostatic functions in the brain [13,25–27]. Astrocytes are the first glial cells directly abutting the basement membranes of the two mural vascular cells (endothelial cells and pericytes) of the NVU in the healthy brain. This places astrocytes in a unique position for connecting the regional cortical neurons to NVU mural cells. It is this connection between the NVU and the neuron that contributes to a local hyperemia when neurons increase their activity. Additionally, astrocytes act as a major supplier of energy via glycogen storage and glycolysis, as well as of antioxidant reserves (glutathione (GSH) and superoxide dismutase (SOD)), growth factors such as brain-derived growth factor transforming growth factor- β and glial-derived growth factor. Astrocytes also define many aspects of synapse formation, plasticity, protective function, synaptic maintenance, and elimination [26,27]. It is important to note, however, that human studies may not always conform to findings in rodents because human protoplasmic astrocytes in the neocortex are much larger and extend longer than in rodent models [28].

In obese, insulin-resistant, and diabetic DBC, we observed the astrocyte end-feet to detach and retract from the basement membrane, which was especially noted when activated microglia cells were actively encompassing or invading the NVU. The normal morphological relationship of the astrocyte with the two vascular mural cells of the NVU (ECs and Pcs) is shown in Figures 1A,B, 3, 4A,B, 5, 6, and 7A,B. Previous images demonstrating AC detachment include Figures 4C,D, 5, and 7C,D. Herein, we provide additional representative observational findings of the activated AC detachment and retraction from the EC and Pc BMs (Figure 8).

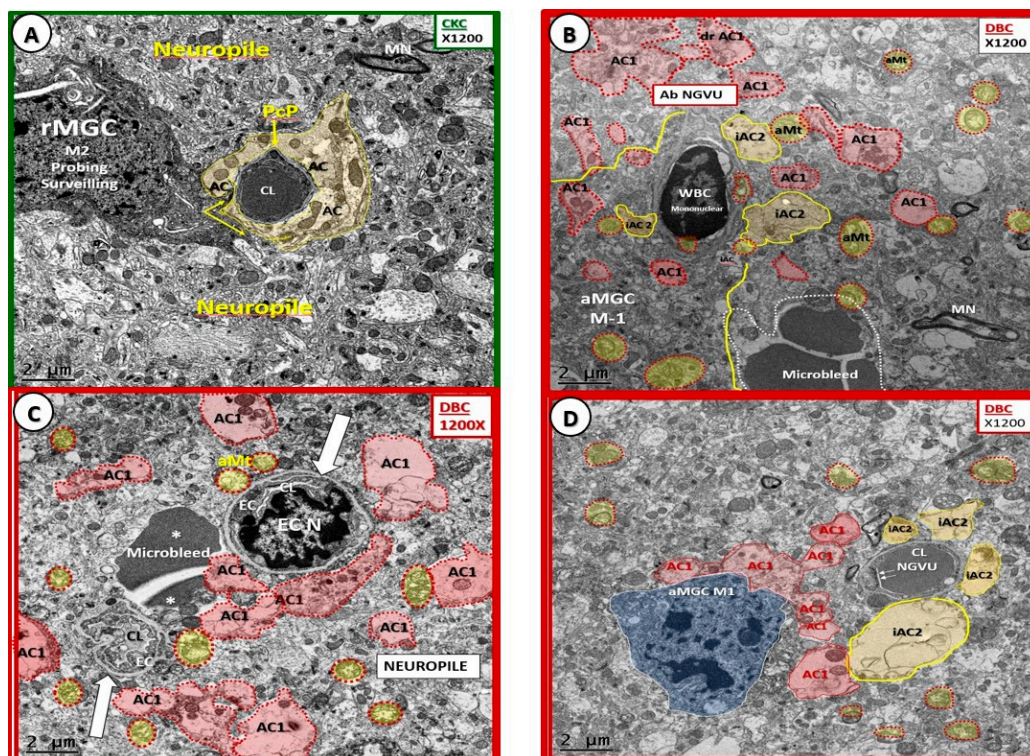


Figure 8. Detachment and retraction of protoplasmic AC in diabetic DBC models. Panel (A) depicts the control (CKC) NVU and note that the “golden halos” (corona of the iAC2) tightly about the NVU EC and Pc BMs. Note the nearby ramified microglial cell that is surveilling the NVU (arrows). In panel (B), there are still three remaining intact type 2 pseudo-colored golden in contrast to the detached and retracted AC-1 (pseudo-colored pink with red outlines). Panel (C) depicts the total loss of iAC2 and all of the ACs having undergone phenotypic polarization to the detached and retracted AC-1-type. Importantly, note the microbleed (asterisks) between the two NVUs (open white arrows), which may

be a contributing factor to the complete absence of the iAC2-type of astrocytes as in the intact AC1 in panel (A). Panel (D) depicts a aMGCM1 phenotype with abnormal nuclear chromatin condensation, which resembles a blue pseudo-colored “frowning face”. The M1 type aMGC may not only contribute to the activation of the polarized-type AC1, but may also result in a structural and possible functional reason for the detachment and retraction of ACs. Indeed, the type 2 iAC2 “golden halos” that used to shine are now gone, detached and retracted from the NVU, and, as a result of their polarized transformation, may contribute to an increased dysfunction and increased permeability of the NVU. Panels (B–D) depict the abnormal detachment and retraction of the AC from the NVU in the diabetic DBC. In panel (B), there are still three remaining iAC2. Incidentally, panel (D) is a lower magnification of Figure 3C. Magnification $\times 1200$; bar = 2 μm . ab NVU—abnormal–aberrant neuroglial vascular unit; MN—myelinated neuron; WBC—monocytic white blood cell.

The large AC cellular presence in the brain and their vast cell–cell communication via gap junctions may be viewed as the brain’s functional syncytium [29]. The relationship among the NVU, EC, Pc, and their shared outer basement membrane, as well as the cell–matrix attachments via dystroglycans and integrins to NVU ACs, are essential for proper homeostasis and function [29–31]. Possible mechanisms that may result in AC detachment and retraction are illustrated in Section 4 (Figure 8).

3.4. Sticky, Adhesive Red Blood Cells in the Neurovascular Unit of Diabetic DBC Mice

Occasionally, red blood cells (RBCs) were observed to be adherent to the endothelial cells of the NVU in the cortical gray matter. These NVUs demonstrated highly electron-dense protein staining adhesion plaques between the RBC and the endothelium, which may contribute to sludging of RBCs and hypoxia (Figure 9).

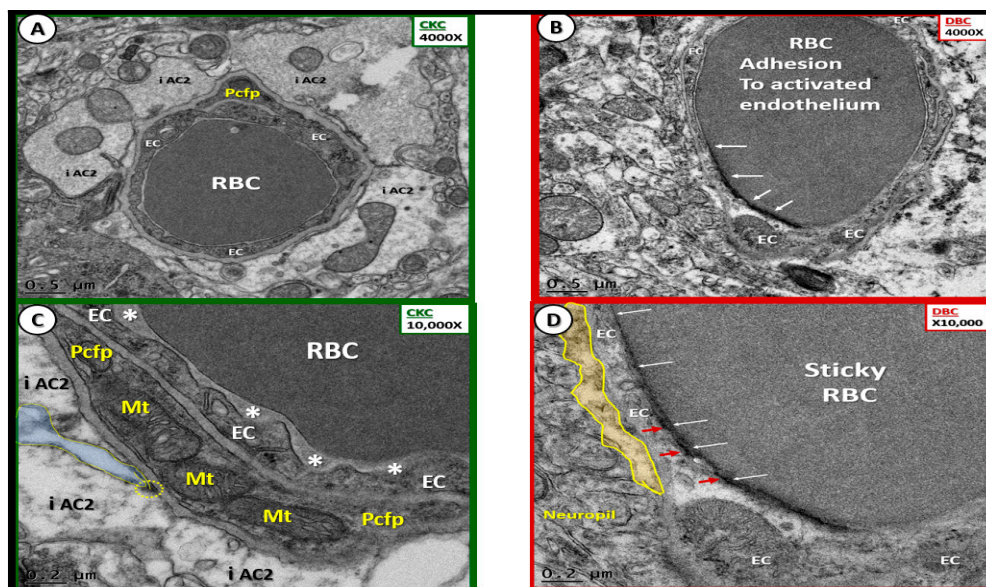


Figure 9. Sticky, adhesive red blood cells (RBCs) in the neurovascular unit of diabetic DBC models. Panels (B,D) depict the presence of a marked electron density between the RBC and the luminal EC (arrows). In panel (D), there appears to be an electron-dense protein staining in the RBC (white arrows) and also the EC (red arrows) that appear to fuse into one continuous electron-dense RBC/EC adhesion plaque. Also note that the ACs are retracted on the left side of the NVU in panel (B). Magnification $\times 4000$ and $\times 10,000$; bar = 0.5 and 0.2 μm , in panels (B,D), respectively. Panels (A,C) illustrate the relationship between the capillary RBC and the ECs without electron-dense adhesive adherence plaques in CKC models. In panel (C), note the compressed endothelial glycocalyx (asterisks), which were not observed in the diabetic NVUs as in panels (B,D). Magnification $\times 4000$ and $\times 10,000$; bar = 0.5 and 0.2 μm , in panels (A,C), respectively. Pcfp—pericyte foot process

While the elusive endothelial glycocalyx was not specifically studied in these models, it was observed to be compressed between the capillary RBCs and the endothelium only in CKC models (Figure 9C). Notably, the endothelial glycocalyx was not observed in the DBC models.

3.5. Neurovascular Unit Microbleeds in the Diabetic DBC Mice

In the DBC cortical gray matter, we found evidence of microbleeds/microhemorrhages, and these regions were associated with very small capillaries ($\leq 2\text{--}3\ \mu\text{m}$) with notable loss of mural supportive Pcs and detached/retracted ACs (Figures 10 and 11).

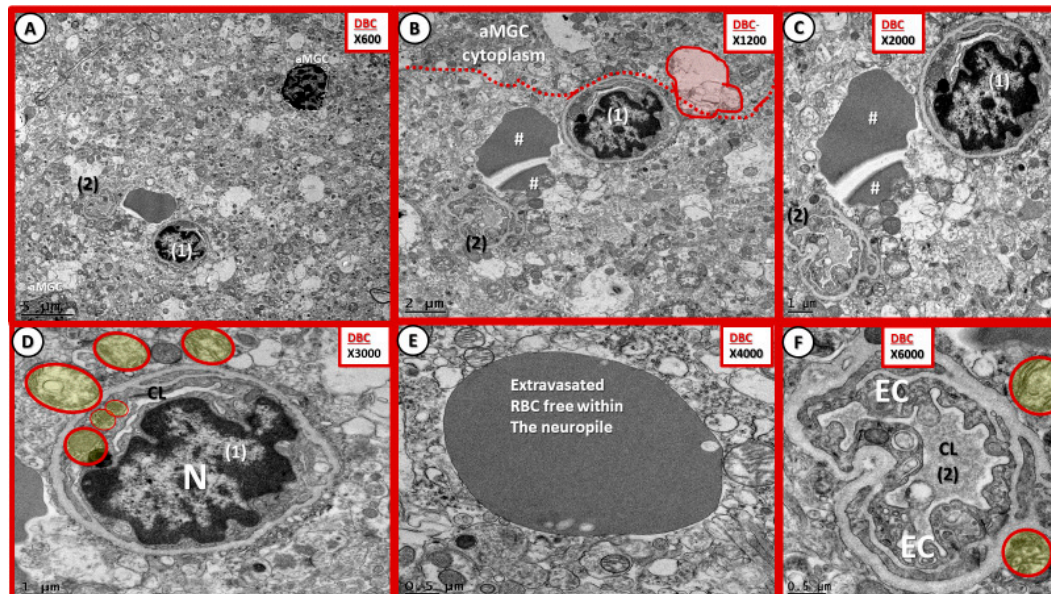


Figure 10. Cortical gray matter microbleeds in diabetic DBC models. Panel (A) illustrates a microbleed between two small NVU capillaries (1) and (2) at low magnification $\times 600$; bar = $5\ \mu\text{m}$. Panel (B) depicts this microbleed (#) in a different region of cortical layer III of the gray matter, and note once again that this microbleed resides between two capillary NVUs (1) and (2). Also, note how the electron-lucent ACs are detached and retracted except for the one colored pink with the encircling solid red line (panel (B)). Magnification $\times 1200$; bar = $2\ \mu\text{m}$. Panel (C) demonstrates the close proximity of the homogenous microbleed (#) to the paired capillary NVUs. Magnification $\times 2000$; bar = $1\ \mu\text{m}$. Panel (D) at higher magnification depicts aMt, which are pseudo-colored yellow with red lines encircling them. Magnification $\times 3000$; bar = $1\ \mu\text{m}$. Panel (E) allows one to appreciate the rounded homogeneous electron staining that appears similar to a red blood cell or plasma that would be normally located within a capillary lumen; however, this is located outside of any capillary lumen, and is totally surrounded by the neuropil. Magnification $\times 4000$; bar = $0.5\ \mu\text{m}$. Panel (F) also demonstrates aMt in the immediate vicinity of a different NVU similar to panel (D), and these aMt may be a result of or contribute to the associated microbleeds. Magnification $\times 6000$; bar = $0.5\ \mu\text{m}$.

3.6. Nanometer Channels as Possible Origins of the Glymphatic Pathway

While this was not our goal in this study, we were able to observe at least one nanometer-sized channel region that may represent an origin of a glymphatic channel in a transitional region from an NVU capillary with a pericyte lining to an early small arteriole, but with a pericyte lining versus a smooth-muscle-cell lining as in a true arteriole (Figure 12). Additionally, we were able to observe at least six nanometer-sized ultrastructure channels at the NVU that appeared to be bounded by the EC and Pc basal lamina and by the protoplasmic astrocyte basal lamina in the control CKC models (Figure 13). Notably, none of these channels were present in the DBC, which may be due to the previously described AC detachment and separation in diabetic DBC models.

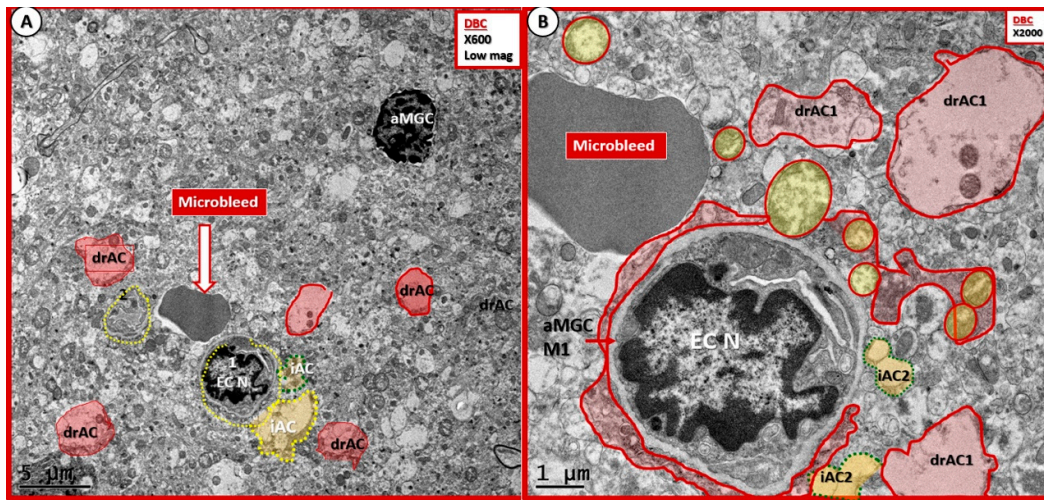


Figure 11. Cortical gray matter microbleeds in diabetic DBC models. Panels (A,B) illustrate the detachment and retraction of reactive-activated ACs (drAC1) in the NVU within the immediate proximity of this microbleed (pseudo-colored pink with red outlines). Note in these images that there is only one intact AC2 (golden colored iAC2) remaining. Also, note the aMt (pseudo-colored yellow with red outlines), which could certainly contribute to increased NVU oxidative stress and could support ongoing EC and AC activation, as depicted. Importantly, note the invasion/infiltration by aMGC (pseudo-colored red with encircling red lines) that are almost totally encompassing this NVU. Magnification $\times 600$; bar = $2 \mu\text{m}$, and $\times 2000$; bar = $1 \mu\text{m}$ (panels (A,B), respectively). EC N—endothelial cell nucleus.

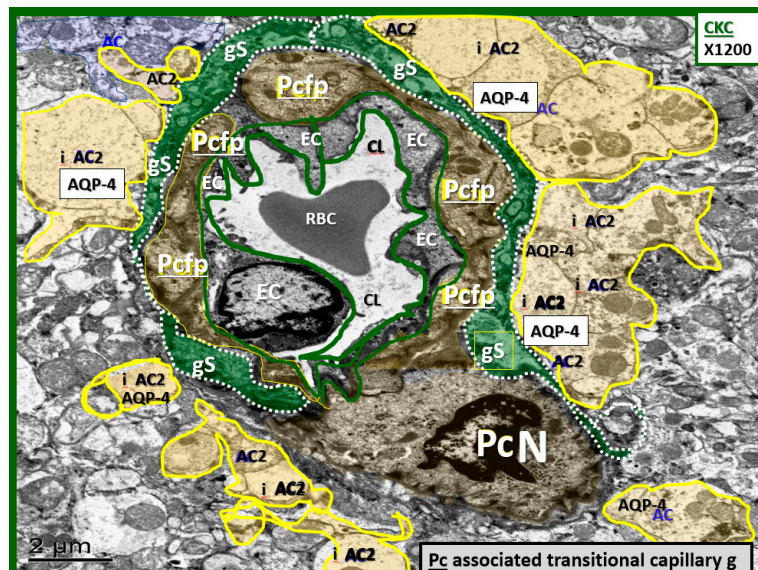


Figure 12. Cortical gray matter NVU capillary may demonstrate a potential paravascular waste clearance channel. This transitional capillary describes one transitioning from a capillary NVU to an arteriole. This NVU capillary EC is still encompassed by a layer of Pcfp with an intact PcN. Between the Pcfp and its basal lamina, and between the surrounding iAC2 and their basal lamina, there is a space that may represent the glymphatic pathway or glymphatic space (gS; pseudo-colored green). This possible glymphatic space may be important for waste clearance from the nanometer channels, and may also represent an ultrastructural origin of the glymphatic pathway in a previous image (Figure 13). The presence of aquaporin 4 (AQP-4) in the basolateral regions of the intact ACs is important for waste clearance. Magnification $\times 1200$; bar = $2 \mu\text{m}$.

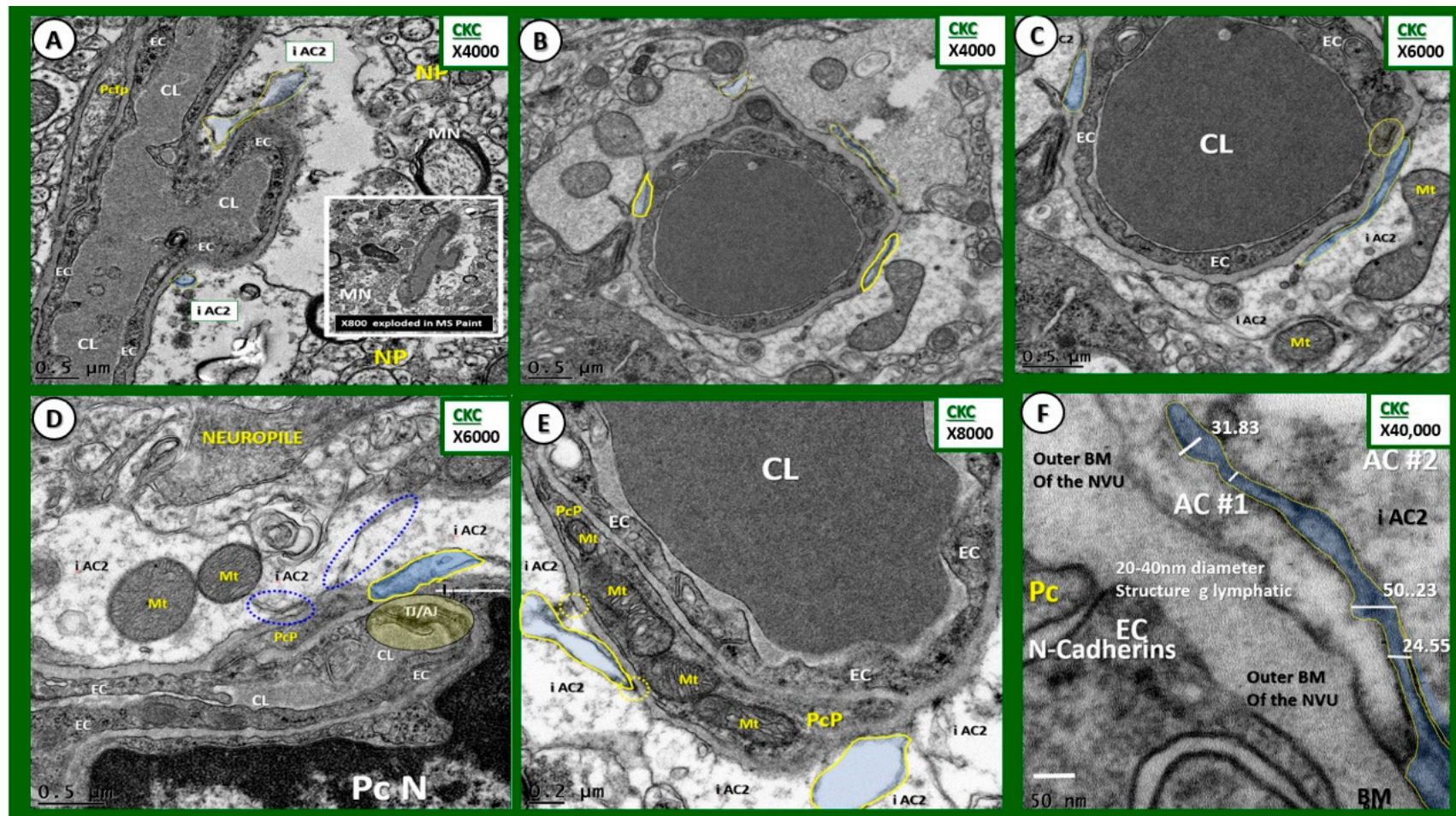


Figure 13. Possible origin of nanometer waste clearance channels adjacent to the NVU in the non-diabetic CKC models. Panels (A–F) illustrate various magnifications of the NVUs with nanometer-sized channels (pseudo-colored blue and outlined by yellow lines) adjacent to EC and Pc BMs. These proposed nanometer waste clearance channels measured 20–50 nm in width, and some were up to 800 nm in length. Magnifications are located in the upper right-hand corner and scale bars in the lower left-hand corner.

4. Discussion

Diabetes-associated cognitive impairment was previously described, and the currently used terminologies include “diabetic encephalopathy”, initially described in 1950 [32], “type three diabetes” in 2008 [33], and “diabetic cognopathy” in 2013 [13].

Since capillaries comprise $\geq 60\%$ of the cerebral microvasculature [31], our initial aim was to characterize the capillary NVUs in obese, insulin-resistant, type 2 diabetic female db/db DBC mouse models, and our observational findings demonstrated abnormal, multi-cellular maladaptive ultrastructural remodeling changes in the NVUs of the mid cortical gray matter regions of the brain. These ultrastructure remodeling changes were not previously described in db/db models to the best of our knowledge; however, they may contribute to impaired cognition in the DBC as described in various papers regarding behavioral testing [34–39]. These cognitive impairments include behavioral testing abnormalities of the db/db models (DBC) in the Morris water maze tests, forced swim test, tail suspension test, light/dark box test, olfactory testing, Y-maze, and open-field tests to evaluate learning and memory plus anxiety and/or depression-associated cognitive impairment/deficits.

Understanding the NVU ultrastructural morphology and how this structure maladaptively remodels in the DBC as compared to the CKC models may allow for a better understanding of how the NVU responds to obesity, insulin resistance, and T2DM. Herein, we found concurrent multicellular maladaptive remodeling in the cells comprising the capillary NVU structures: (i) endothelial cell BBB TJ/AJ; (ii) endothelial cell luminal contents (sticky RBCs) and extraluminal microbleeds; (iii) pericytes; (iv) BM thickening in the NVU (ECs and encompassed Pcs); (v) astrocytes.

- i. Endothelial cell BBB TJ/AJ attenuation and/or loss would allow increased permeability (due to dysfunction, attenuation, and/or loss of its permeability barrier), which would allow the accumulation of multiple vasculotoxic and neurotoxic moieties within the NVU parenchyma (Figures 3B–D, 4C,D, 5, 7C,D, 8, and 9) [6]. This compromise of the EC BBB TJ/AJ may aid in the understanding as to why there is concurrent remodeling in the surrounding cellular and extracellular regional constituents of the NVU. Importantly, these ultrastructural maladaptive remodeling changes could also interfere with neurovascular signaling/coupling functions of astrocytes to both pericytes and endothelial cells, which could lead to dysfunction and/or loss of function. As a result, there could also be a reduction in regional cerebral blood flow with regional hypoperfusion and ischemia [4–8].
- ii. Luminal RBCs were observed to become adherent (via adherence plaques) in DBC models, which were not observed in the CKC models (Figure 10). Red blood cells become excessively glycosylated and form advanced glycation end products (AGE) with hemoglobin in human and DBC models of T2DM. Previously, our group showed elevations of hemoglobin A1c (HbA1c) [21], which is known to increase RBC stiffness that is associated with the loss of RBC deformability [40]. The accumulation of AGE in the RBC outer plasma membrane regions will serve as a ligand to the EC AGE receptor (RAGE). Additionally, the inner plasma membrane may translocate phosphatidylserine (PS) to the outer leaflet in the hyperglycemic microenvironment of DBC models. The translocated or “flipped” outer leaflet PS will contribute to the adherence of RBCs to the EC PS receptor, as well as to the EC matrix of thrombospondin, $\alpha v \beta 1$, and CD36, which may add to the increased electron density of the proteinaceous electron-dense adhesion plaques of the RBC and EC [41,42]. Importantly, there were also adherent mononuclear white blood cells within the capillary lumen of NVUs observed in the cortical gray matter in DBC models, as depicted in previous figures (Figures 4C,D, 7C and 8B), which will be discussed in greater detail as they relate to microglia remodeling. While the elusive endothelial glycocalyx was not specifically studied in this experiment, it is known that hyperglycemia results in the loss or shedding of the protective endothelial glycocalyx, and thus, may result in a more vulnerable and activated endothelium with increased inflammation and injury, decreased endothelial bioavailability of

- nitric oxide, and impaired vasodilation, in addition to becoming a more pro-coagulant surface in the DBC models (Figure 10C,D) [43].
- ii. Microbleeds/microhemorrhages within the gray matter of the cortical layers were observed in DBCs, which certainly could be related to incompetent EC TJ/AJ BBB proteins. These hemoglobin-containing extrusions/microbleeds would contain iron that could promote additional oxidative stress to the NVU and the immediate surrounding tissues (Figures 11 and 12). Importantly, RBC remodeling can result in increasing dysfunction and/or damage to the NVU as a result of adherence, escaping, or loss of deformability within NVU capillary lumen in DBC models. Of note, cerebral microbleeds are being increasingly found on magnetic resonance imaging (MRI) [44]. Currently, the significance of microbleeds in diabetic preclinical models is yet to be evaluated extensively at the transmission electron microscopic ultrastructural level; however, there may be some similarities to retinal microbleeds and hemorrhages [45]. Notwithstanding, these observed microbleeds may be related to remodeled and dysfunctional TJ/AJ. The combination of adherent RBCs and microbleeds in the DBC may have detrimental consequences in local regional blood flow with resultant regional ischemia and loss of neurovascular coupling in the DBC models and may have a predisposition to accelerated neurodegeneration.
 - iii. Maladaptive Pc remodeling (Figure 7) in diabetes may contribute to increased BBB TJ/AJ permeability, neuronal dysfunction, injury, and eventual neurodegeneration [13,15,18,25]. Recently, in streptozotocin-induced type 1 diabetes, it was demonstrated that pericytes are also attenuated and/or lost, and that the mitochondrial-specific carbonic anhydrase inhibitor (toprimate) was able to rescue pericyte loss and normalise BBB permeability [46]. Our findings of aberrant mitochondria in DBC pericytes may be playing a detrimental role in our observed pericyte attenuation and/or loss (Figure 7E).
 - iv. Capillary NVU BM thickening was observed in the cortical gray matter of DBC ($\sim \geq 200$ nm) as compared to the CKC ($\sim \leq 80$ nm) models (Figures 4 and 5). Capillary BM thickening is a fundamental ultrastructural central finding in most diabetic affected end-organs and nearly a pathognomonic ultrastructural finding in human and rodent models of diabetes. Capillary NVU BM thickening was reported in human diabetics in the cortical regions of the brain [47]. Basement membrane thickening was also reported in the retinas of type 1 diabetic rats (streptozotocin-induced) at six months of age [48], whereas we did not observe BM thickening in our type 1 diabetic mice mid-brain models studied at four months in a previous study [18]. Mechanisms of BM thickening may be related to glucotoxicity, increased protein kinase C, increased vascular endothelial cell growth factor, increased AGE, type IV collagen AGE crosslinking, and oxidative stress [23]. The observed increase in BM thickness may increase NVU permeability and could also play a role in the detachment of ACs from the capillary EC and Pc NVU BM due to an interference in cell-matrix interactions and dysfunctional alterations of BM integrins/dystroglycans. The current finding of BM thickening in DBC models filled in some gaps in our knowledge regarding the lack of BM thickening in diet-induced obesity Western mice models (cortical gray matter) [13] and the type 1 diabetic mice models previously studied (cortical mid-brain) [23]. To the best of our knowledge, we are the first to identify BM thickening in capillary EC/Pc NVU microvessels in the cortical gray matter of the female obese, insulin-resistant, type 2 diabetic db/db mouse model.
 - v. Abnormal remodeling changes of the supportive and connecting protoplasmic astrocytes were observed in the DBC models. Astrocytes foot processes were depicted in CKC images as being colored “golden” due to their important function and location as connecting cells between the capillary NVU and their regional neurons when they were observed to have intact connections with the EC and Pc basement membranes. We observed how these connecting intact astrocytes became detached and retracted from the capillary EC and Pc BMs in the DBC, and how they lost their connective essential role of neurovascular coupling. This loss of neurovascular coupling

and loss of vasodilation when being actively signaled by regional neurons could result in a loss of function that could result in localized decreased cerebral blood flow, resulting in regional hypoxia with the potential for increased neurodegeneration. In the detached astrocyte, it is possible that the AC soma may remodel its F-actin cytoskeleton such that the AC protoplasmic processes retract toward the soma of the AC in a phenotypic response to injury (brain wounding mechanism), which may result from a combination of excessive reactive oxygen/nitrogen species, toxic cytokines, and ischemia in the DBC models. Some suggested that the activated-reactive detached AC are induced by activated microglia cells [49–51], and furthermore, that these activated microglia may be responsible for the actual physical detachment and subsequent retraction of the capillary NVU astrocytes in the DBC (Figure 4C,D and Figure 5).

Possible mechanisms of astrocyte detachment and retraction may include the invading reactive-aMGC (Figure 14). The aMGCs may physically result in a shearing (bulldozer-like effect) as they invade the NVU, which may result in the physical detachment of ACs. Importantly, these invading aMGCs are known to be capable of secreting excess toxic reactive oxygen/nitrogen species (ROS and oxidative/nitrosative stress) due to the actions of excessive nicotinamide adenine dinucleotide phosphate (NADPH) oxidase and toxic cytokines, which are capable of activating local EC proteolytic matrix metalloproteinases, such as MMP-2. Also, hyperglycemia and resultant excess protein kinase C, ROS production via glucose autoxidation, AGE-RAGE interactions, polyol, and hexosamine flux pathways in the EC will be capable of increasing ROS production. In turn, this excess ROS will further increase not only matrix metalloproteinases (MMP-2) production by ECs, but also inducible (MMP-9) activation by surrounding Pcs and ACs. These above mechanisms may be synergistic with the observed attenuation and/or loss of EC BBB TJ/AJ and pericytes. The detachment and retraction of astrocytes may provide new insights into the loss of neurovascular coupling and eventual neurodegeneration in the DBC (Figure 14).

Early on, the brain was known to lack a classical endothelial-lined lymphatic system as described in the peripheral tissues, and a specific lymphatic-like pathway channel remained somewhat elusive. Recently, the presence of a new paravascular lymphatic pathway/system was described [50–52]. The “g” preceding the word lymphatic, or “glymphatic”, is to honor the importance of the glial ACs and their important polarized water channel, aquaporin-4, which is localized to the basal lateral position of ACs that abut and line the EC and Pc basement membranes. Importantly, others suggested that these paravascular channels may potentially extend all the way to the capillary level of the NVU [53]. Concurrent with the above findings, other groups identified lymphatic channels in the meninges, and suggested that the drainage was accomplished via a “perivascular channel” that moves within the basal lamina regions of the outer arteriole smooth muscle cells and adventitia [54]. Of interest, another paper recently discussed the current understanding, significance, and controversy of these waste clearance pathways [55].

A timely publication was released during the preparation of this manuscript (May 2018) regarding the entrance of a cerebral spinal fluid (CSF) tracer (soluble, fluorescent fixable amyloid β ($A\beta$)) that was introduced via the cisterna magna. These findings demonstrated that the tracer entered the brain along the pial-glial BMs, and reasons for its entry into the extracellular matrix interstitial fluid was not completely clear; however, authors stated there could be multiple reasons [56]. The mixture of the interstitial spinal fluid and CSF was then found to enter the BM regions in capillary walls, before draining further into the BMs of vascular smooth muscle cells within the tunica media in the pial arterioles and arteries within the intramural peri-arterial drainage pathways to the sagittal sinus and cerebral spinal fluid. Also demonstrated in this study was the finding that injected tracers were found to enter and leave the brain along separate peri-arterial basement-membrane pathways [56].

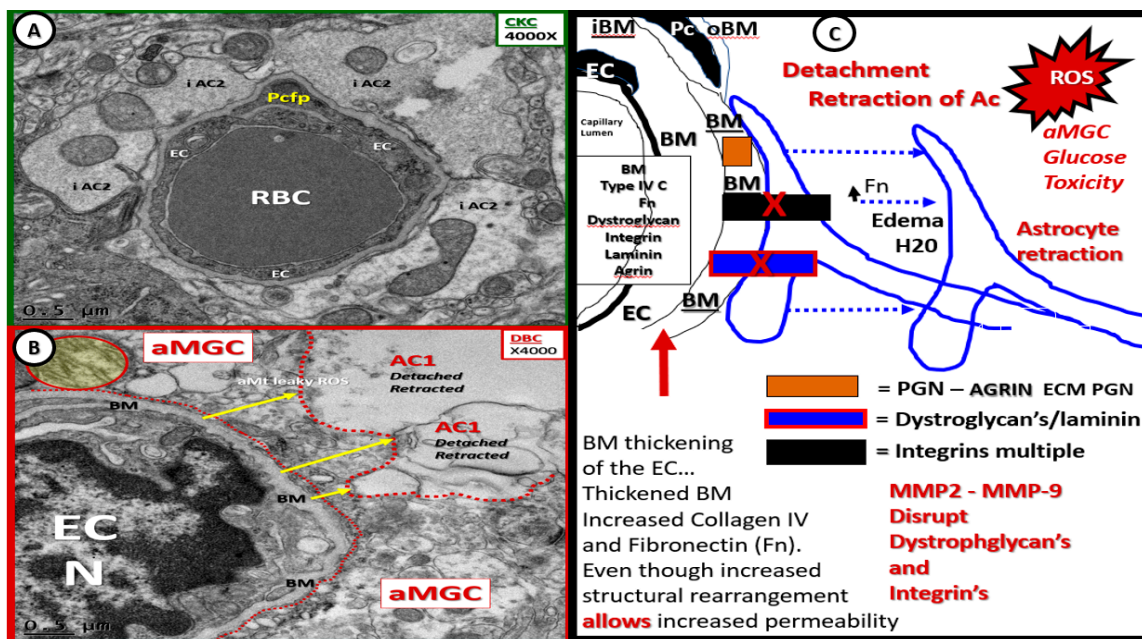


Figure 14. Possible mechanisms for detachment and retraction of astrocytes in diabetic DBC. Panel (A) demonstrates the iAC2 in the CKC. Panel (B) depicts the near complete loss of iAC2 coverage of the EC and Pcfp. Importantly, note the detachment and retraction (yellow arrows) of phenotypically retracted ACs, labeled AC1, in the DBC. Note the aberrant mitochondria in this image in the detachment zone (pseudo-colored yellow and outlined by red solid line). Also, note the aMGC that is located between the NVU EC BM and the detached AC1 (red dashed lines). Magnification $\times 4000$; scale bar = $0.5 \mu\text{m}$. Panel (C) contains a cartoon, which may illustrate some of the possible involved mechanisms. C—collagen IVECM—extracellular matrix; Fn—fibronectin; H2O—water-edema; MMP2-9—matrix metalloproteinases 2-9; PGN—proteoglycan; ROS—reactive oxygen/nitrogen species.

Interestingly, possible nanometer spaces/channels were observed in both the capillary NVU regions and in pre-arteriole transitional pericyte-lined microvessels of the non-diabetic CKC models (Figures 13 and 14), which were not observed in the diabetic DBC. Whether this is due in part to the outer wall AC detachment and retraction from NVU EC and Pc BMs or the immersion-fixation process utilized in this model remains to be studied in greater detail. It is not certain that these shared images will assist in making any headway or advances; however, they support the discussion that the “glymphatic pathway” may actually have its origin at the capillary NVU to begin the clearance of metabolic toxic waste products from the interstitial fluid of the brain, as seen in Figure 1a that Abbott et al. [53] shared.

The puzzling mechanisms for the clearance of waste products via a specialized glymphatic system of the brain are still far from being completely elucidated, and it may be eventually demonstrated that both the perivascular and paravascular routes for clearance of metabolic byproducts and toxic oligomers of $A\beta$ and other proteins may be cleared via a little bit of both systems currently described in the literature. Regardless, when ACs are detached and retracted from the NVU (in addition to other cellular remodeling changes as found in the cortical gray matter NVUs of DBC models), these changes may result in impaired waste clearance in the DBC models.

Certain limitations apply to this study, which include the following: (i) this study was limited to immersion fixation, which studied only a snap shot in time; however, these images allowed comparisons at the same point in time between healthy normal controls (CKC) and diabetic (DBC), such that maladaptive remodeling changes could be observed; (ii) this study was limited to the cortical gray matter (primarily layer III) and may not apply to other regions of the brain such as the hippocampus, mid-brain, or cerebellum. However, cortical remodeling usually occurs at later time

points than hippocampal remodeling, and therefore, may be representative of earlier time points in the expectation of similar remodeling findings in the hippocampal structure); (iii) this study was primarily designed and directed to interrogate the NVU and its immediate surroundings; (iv) this study was limited to only ultrastructural observational findings, and was not supported by functional studies, immunohistochemistry, or protein Western blots. As with any transmission electron microscopic study, the regions studied were very small and limited. Furthermore, this study was not supported by larger regions of study, such as light microscopy, to more closely examine larger areas of tissue remodeling. In general, the above limitations reflect the very nature of TEM studies in general when not accompanied by other functional and light microscopic methods. Given these limitations, however, this study does allow for the ultrastructural comparisons of age-matched CKC to the diseased obese, insulin-resistant, and diabetic DBC at the same time points. Additionally, the authors attempted referencing what other investigators previously established in diabetic models.

While each individual cellular component of the NVU is considered to be a vital element to ensure proper functioning, homeostasis, and integrity, the multicellular remodeling in the brains of the DBC are thought to be of extreme interest. The detachment and retraction of the ACs from the capillary NVUs are thought to be very important novel findings, in that, ACs are the connecting/communicating cell between the regional neurons and capillary microvessels of the NVU, providing neurovascular coupling. This loss of neurovascular coupling could possibly provide novel mechanisms for impaired regional capillary blood flow, cerebral blood flow dynamics, and regional ischemia, which may markedly contribute to the ongoing neurodegenerative progression in this model and the increased vulnerability to age-related neurodegenerative diseases.

The authors observed that, in most of the diabetic end-organs affected by T2DM, there appears to be accelerated/premature aging. These observations suggest that T2DM may induce premature macrovascular and microvascular brain aging and/or negatively interact with the normal aging process [57], which supports the brain reserve hypothesis [58]. Accelerated aging could render these cells highly vulnerable to the effects of other specific neurologic age-related diseases, such as Alzheimer's disease, vascular dementia, and Parkinson's disease. Indeed, other investigators also suggested that T2DM is associated with learning and memory dysfunction, specifically in older adults [59].

In summary, to the best of our knowledge, we are the first group to perform an in-depth ultrastructural study of the brain NVU in obese, insulin-resistant, and diabetic female db/db DBC models with the transmission electron microscope. Ultrastructural observations included an attenuation and/or loss of EC BBB TJ/AJ and Pc, as hypothesized, as well as capillary NVU BM thickening and abnormal remodeling in supportive neuroglia ACs, consisting of detachment and retraction from the NVUs. Also, there were observational findings of sticky red blood cells and microbleeds in the DBC that were not noted in CKC. Additionally, we were not only able to image a possible example of the recently defined glial lymphatic (glymphatic) pathway system at the CKC pre-arteriolar and capillary NVU level, but we were also able to demonstrate a possible nanoscale origin of the glymphatic system for waste clearance.

These observational findings, in whole or in part, appear important to the known impaired cognition in db/db models of T2DM, and certainly suggest that the multicellular remodeling may place a certain credence regarding the saying that the whole may be greater than the sum of its parts. Indeed, this study was certainly a voyage of discovery, and while we may all dance around in a ring and suppose, the secret sits in the middle and knows ("The Secret Sits"—a poem by Robert Frost (1874–1963)). These sage thoughts by Frost suggest that the abnormal cellular remodeling changes may represent the secret sitting in the middle in order for us to better understand the complicated structures of the brain in the diabetic DBC as compared to the control CKC models.

5. Type 2 Diabetes Mellitus Increases the Risk of the Neurodegenerative Diseases, Alzheimer's and Parkinson's Disease

Type 2 diabetes mellitus is known to increase the risk of developing AD. However, the increased clinical risk that T2DM brings to the development of PD was only recently more strongly established during the preparation of this manuscript [60]. Our observational ultrastructural findings of the NVU in T2DM DBC models are quite disturbing, in that, these maladaptive remodeling changes of the NVU in DBC models could lead to predisposition to additional maladaptive remodeling with aging, and the increased vulnerability of the T2DM brain tissue to age-related neurodegenerative diseases.

6. Future Directions

Now that there is an established model of marked ultrastructural remodeling changes in the NVU in the female diabetic DBC, studies utilizing various treatment modalities are certainly of great interest. Multiple treatment modalities may be studied to observe if they can prevent/abrogate the ultrastructural brain remodeling. Additionally, functional studies utilizing light microscopy, immunohistochemistry, and protein and mechanistic studies may be employed. Also, there are newer technologies being utilized even currently, and of course, newer technologies that are yet to be created in the future.

One exciting new modality in current use is the focused ion beam/scanning electronic microscopic (FIB/SEM) instrument [61] that is being increasingly incorporated in core facilities to capture images (Figure 15).

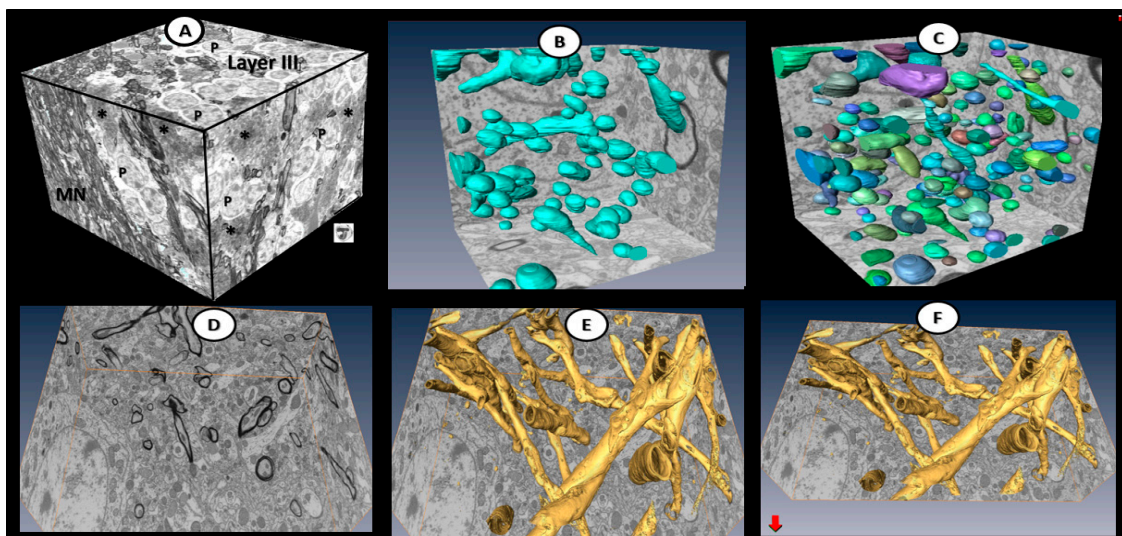


Figure 15. Examples utilizing focused ion beam/scanning electronic microscopic (FIB/SEM) technology to study various models of disease. Panel (A) illustrates the use of 3-view system (Gatan, Inc., Pleasanton, CA, USA) with tagged image file format (TIFF) cutouts in diet-induced obesity models of cortical gray matter layer III (P—pyramidal cells; MN). Panels (B–D) were obtained by utilizing FIB/SEM technology. Panels (B,C) depict randomized pseudo-colored Mt in control CKC models. Panels (D–F) demonstrate myelin. In panel (D), note that the myelin is not pseudo-colored, in contrast to panels (E,F), where the myelin is pseudo-colored golden in control CKC models. No specific magnification or actual scale bars are included in these FIB/SEM images.

Some of the potential capabilities of FIB/SEM technology are actually reminiscent of how computerized axial tomography and MRI technologies expanded some of our most recent new findings and concepts regarding both rodent models and human diseases. Regarding brain barriers and fluid movement, a recent paper commented that there are several ongoing clinical trials underway testing

the intrathecal route of drug delivery, which may evolve to become a treatment modality for brain diseases [62]. Indeed, these are exciting times.

Author Contributions: M.R.H. and V.G.D. conceptualized the study; M.R.H. performed the image collection and interpretation; D.G.G. prepared the tissue specimens for transmission electron microscopic studies and assisted M.R.H.; M.R.H. prepared the manuscript; A.R.A. collected tissue specimens; V.G.D., A.R.A., and D.G.G. assisted in editing.

Funding: This study was supported by an integral grant in Excellence in Electron Microscopy grant issued by the University of Missouri Electron Microscopy Core and Office of Research. No external funding was available.

Acknowledgments: Authors wish to thank Tommi White of the University of Missouri Electron Microscopy Core Facility. Authors also wish to thank our mentor James R. Sowers, who inspired us to interrogate, characterize, and understand the secrets that the tissues behold.

Conflicts of Interest: The authors declare no conflict of interest.

References

1. Wild, S.; Roglic, G.; Green, A.; Sicree, R.; King, H. Global prevalence of diabetes: Estimates for the year 2000 and projections for 2030. *Diabetes Care* **2004**, *27*, 1047–1053. [[CrossRef](#)] [[PubMed](#)]
2. Ott, A.; Breteler, M.M.; van Harskamp, F.; Claus, J.J.; van der Cammen, T.J.; Grobbee, D.E.; Hofman, A. Prevalence of Alzheimer's disease and vascular dementia: Association with education. The Rotterdam study. *BMJ* **1995**, *310*, 970–973. [[CrossRef](#)] [[PubMed](#)]
3. Reeve, A.; Simcox, E.; Turnbull, D. Ageing and Parkinson's disease: Why is advancing age the biggest risk factor? *Ageing Res. Rev.* **2014**, *14*, 19–30. [[CrossRef](#)] [[PubMed](#)]
4. Nelson, A.R.; Sweeney, M.D.; Sagare, A.P.; Zlokovic, B.J. Neurovascular dysfunction and neurodegeneration in dementia and Alzheimer's disease. *Biochim. Biophys. Acta* **2016**, *1862*, 887–900. [[CrossRef](#)] [[PubMed](#)]
5. Snyder, H.M.; Corriveau, R.A.; Craft, S.; Faber, J.E.; Greenberg, S.M.; Knopman, D.; Lamb, B.T.; Montine, T.J.; Nedergaard, M.; Schaffer, C.B.; et al. Vascular contributions to cognitive impairment and dementia including Alzheimer's disease. *Alzheimer's Dement.* **2015**, *11*, 710–717. [[CrossRef](#)] [[PubMed](#)]
6. Zlokovic, B.V. Neurovascular pathways to neurodegeneration in Alzheimer's disease and other disorders. *Nat. Rev. Neurosci.* **2011**, *12*, 723–738. [[CrossRef](#)] [[PubMed](#)]
7. Iadecola, C. The pathobiology of vascular dementia. *Neuron* **2013**, *80*, 844–866. [[CrossRef](#)] [[PubMed](#)]
8. Kisler, K.; Nelson, A.R.; Montagne, A.; Zlokovic, B.V. Cerebral blood flow regulation and neurovascular dysfunction in Alzheimer disease. *Nat. Rev. Neurosci.* **2017**, *18*, 419–434. [[CrossRef](#)] [[PubMed](#)]
9. Rocca, W.A.; Petersen, R.C.; Knopman, D.S.; Herbert, L.E.; Evans, D.A.; Hall, K.S.; Gao, S.; Unverzaw, F.W.; Langa, K.M.; Larson, E.B.; et al. Trends in the incidence and prevalence of Alzheimer's disease, dementia, and cognitive impairment in the United States. *Alzheimer's Dement.* **2011**, *7*, 80–93. [[CrossRef](#)] [[PubMed](#)]
10. Leibson, C.L.; Rocca, W.A.; Hanson, V.A.; Cha, R.; Kokmen, E.; O'Brien, P.C.; Palumbo, P.J. Risk of dementia among persons with diabetes mellitus: A population-based cohort study. *Am. J. Epidemiol.* **1996**, *145*, 301–308. [[CrossRef](#)]
11. Ott, A.; Stolk, R.P.; van Harskamp, F.; Pols, H.A.; Hofman, A.; Breteler, M.M. Diabetes mellitus and the risk of dementia: The Rotterdam Study. *Neurology* **1999**, *53*, 1937–1942. [[CrossRef](#)] [[PubMed](#)]
12. Peila, R.; Rodriguez, B.L.; Launer, L.J. Type 2 diabetes, APOE gene, and the risk for dementia and related pathologies: The Honolulu-Asia Aging Study. *Diabetes* **2002**, *51*, 1256–1262. [[CrossRef](#)] [[PubMed](#)]
13. Hayden, M.R.; Banks, W.A.; Shah, G.N.; Gu, Z.; Sowers, J.R. Cardiorenal metabolic syndrome and diabetic cognopathy. *Cardiorenal Med.* **2013**, *3*, 265–282. [[CrossRef](#)] [[PubMed](#)]
14. McConnell, H.L.; Kersch, C.N.; Woltjer, R.L.; Neuwelt, E.A. The Translational Significance of the Neurovascular Unit. *J. Biol. Chem.* **2017**, *292*, 762–770. [[CrossRef](#)] [[PubMed](#)]
15. Hall, C.N.; Reynell, C.; Gesslein, B.; Hamilton, N.B.; Mishra, A.; Sutherland, B.A.; O'Farrell, F.M.; Buchan, A.M.; Lauritzen, M.; Attwell, D. Capillary pericytes regulate cerebral blood flow in health and disease. *Nature* **2014**, *508*, 55–60. [[CrossRef](#)] [[PubMed](#)]
16. Mishra, A.; Reynolds, J.P.; Chen, Y.; Gourine, A.V.; Rusakov, D.A.; Attwell, D. Astrocytes mediate neurovascular signaling to capillary pericytes but not to arterioles. *Nat. Neurosci.* **2016**, *19*, 1619–1627. [[CrossRef](#)] [[PubMed](#)]

17. Petzold, G.C.; Murthy, V.N. Role of astrocytes in neurovascular coupling. *Neuron* **2011**, *71*, 782–797. [[CrossRef](#)] [[PubMed](#)]
18. Salameh, T.S.; Shah, G.N.; Price, T.O.; Hayden, M.R.; Banks, W.A. Blood-brain barrier disruption and neurovascular unit dysfunction in diabetic mice: Protection with the mitochondrial carbonic anhydrase inhibitor topiramate. *J. Pharmacol. Exp. Ther.* **2016**, *359*, 452–459. [[CrossRef](#)] [[PubMed](#)]
19. Hu, G.; Jousilahti, P.; Bidel, S.; Antikainen, R.; Tuomilehto, J. Type 2 diabetes and the risk of Parkinson's disease. *Diabetes Care* **2007**, *30*, 842–847. [[CrossRef](#)] [[PubMed](#)]
20. Butt, A.; Mihaila, D.; Verkhatsky, A. Neuroglia: A New Open-Access Journal Publishing All Aspects of Glial Research. *Neuroglia* **2018**, *1*, 1. [[CrossRef](#)]
21. Habibi, J.; Aroor, A.R.; Sowers, J.R.; Jia, G.; Hayden, M.R.; Garro, M.; Barron, B.; Mayoux, E.; Rector, R.S.; Whaley-Connell, A.; et al. Sodium glucose transporter-2 (SGLT-2) inhibition with empagliflozin improves cardiac diastolic function in a female rodent model of diabetes. *Cardiovasc. Diabetol.* **2017**, *16*, 9. [[CrossRef](#)] [[PubMed](#)]
22. Laws, K.R.; Irvine, K.; Gale, T.M. Sex differences in cognitive impairment in Alzheimer's disease. *World J. Psychiatry* **2016**, *6*, 54–65. [[CrossRef](#)] [[PubMed](#)]
23. Hayden, M.R.; Sowers, J.R.; Tyagi, S.C. The central role of vascular extracellular matrix and basement membrane remodeling in metabolic syndrome and type 2 diabetes: The matrix preloaded. *Cardiovasc. Diabetol.* **2005**, *4*, 9. [[CrossRef](#)] [[PubMed](#)]
24. Thomsen, M.S.; Routhe, L.J.; Moos, T. The vascular basement membrane in the healthy and pathological brain. *J. Cereb. Blood Flow Metab.* **2017**, *37*, 3300–3317. [[CrossRef](#)] [[PubMed](#)]
25. Bell, R.D.; Winkler, E.A.; Sagare, A.P.; Singh, I.; LaRue, B.; Deane, R.; Zlokovic, B.V. Pericytes control key neurovascular functions and neuronal phenotype in the adult brain and during brain aging. *Neuron* **2010**, *68*, 409–427. [[CrossRef](#)] [[PubMed](#)]
26. Verkhatsky, A.; Nedergaard, M. Astroglial cradle in the life of the synapse. *Phil. Trans. R. Soc. Lond. B Biol. Sci.* **2014**, *369*, 20130595. [[CrossRef](#)] [[PubMed](#)]
27. Verkhatsky, A.; Nedergaard, M. Physiology of Astroglia. *Physiol. Rev.* **2018**, *98*, 239–389. [[CrossRef](#)] [[PubMed](#)]
28. Verkhatsky, A.; Bush, N.A.; Nedergaard, M.; Butt, A. The Special Case of Human Astrocytes. *Neuroglia* **2018**, *1*, 4. [[CrossRef](#)]
29. Scemes, E.; Spray, D.C. Chapter: The astrocytic syncytium. In *Non-Neural Cells in the Nervous System: Function and Dysfunction*; Hertz, L., Ed.; Elsevier: New York, NY, USA, 2004; Volume 31, pp. 165–179.
30. Abbott, N.J.; Rönnbäck, L.; Hansson, E. Astrocyte-endothelial interactions at the blood-brain barrier. *Nat. Rev. Neurosci.* **2006**, *7*, 41–53. [[CrossRef](#)] [[PubMed](#)]
31. Del Zoppo, G.J.; Milner, R. Integrin–Matrix Interactions in the Cerebral Microvasculature. *Arterioscler. Thromb. Vasc. Biol.* **2006**, *26*, 1966–1975. [[CrossRef](#)] [[PubMed](#)]
32. Reske-Nielsen, E.; Lundbaek, K. Diabetic Encephalopathy. In *Pathophysiologie und Klinik/Pathophysiology and Clinical Considerations*; Pfeiffer, E.F., Ed.; Springer: Berlin/Heidelberg, Germany, 1971.
33. De la Monte, S.M.; Wands, J.R. Alzheimer's Disease Is Type 3 Diabetes—Evidence Reviewed. *J. Diabetes Sci. Technol.* **2008**, *2*, 1101–1113. [[CrossRef](#)] [[PubMed](#)]
34. Li, X.L.; Aou, S.; Oomura, Y.; Hori, N.; Fukunaga, K.; Hori, T. Impairment of long-term potentiation and spatial memory in leptin receptor-deficient rodents. *Neuroscience* **2002**, *113*, 607–615. [[CrossRef](#)]
35. Zheng, H.; Zheng, Y.; Zhao, L.; Chen, M.; Bai, G.; Hu, Y.; Hu, W.; Yan, Z.; Gao, H. Cognitive decline in type 2 diabetic db/db mice may be associated with brain region-specific metabolic disorders. *Biochim. Biophys. Acta* **2017**, *1863*, 266–273. [[CrossRef](#)] [[PubMed](#)]
36. Ramos-Rodriguez, J.J.; Ortiz, O.; Jimenez-Palomares, M.; Kay, K.R.; Berrocoso, E.; Murillo-Carretero, M.I.; Perdomo, G.; Spires-Jones, T.; Cozar-Castellano, I.; Lechuga-Sancho, A.M.; et al. Differential central pathology and cognitive impairment in pre-diabetic and diabetic mice. *Psychoneuroendocrinology* **2013**, *38*, 2462–2475. [[CrossRef](#)] [[PubMed](#)]
37. Andersen, J.V.; Nissen, J.D.; Christensen, S.K.; Markussen, K.H.; Waagepetersen, H.S. Impaired Hippocampal Glutamate and Glutamine Metabolism in the db/db Mouse Model of Type 2 Diabetes Mellitus. *Neural Plast.* **2017**, *2017*, 2107084. [[CrossRef](#)] [[PubMed](#)]
38. Ernst, A.; Sharma, A.N.; Elased, K.M.; Guest, P.C.; Rahmoune, H.; Bahn, S. Diabetic db/db mice exhibit central nervous system and peripheral molecular alterations as seen in neurological disorders. *Transl. Psychiatry* **2013**, *3*, e263. [[CrossRef](#)] [[PubMed](#)]

39. Kalani, A.; Chaturvedi, P.; Maldonado, C.; Bauer, P.; Joshua, I.G.; Tyagi, S.C.; Tyagi, N. Dementia-like pathology in type-2 diabetes: A novel microRNA mechanism. *Mol. Cell. Neurosci.* **2017**, *80*, 58–65. [[CrossRef](#)] [[PubMed](#)]
40. Tomaiuolo, G. Biomechanical properties of red blood cells in health and disease towards microfluidics. *Biomicrofluidics* **2014**, *8*, 051501. [[CrossRef](#)] [[PubMed](#)]
41. Carelli-Alinovi, C.; Misiti, F. Erythrocytes as Potential Link between Diabetes and Alzheimer's Disease. *Front. Aging Neurosci.* **2017**, *9*, 276. [[CrossRef](#)] [[PubMed](#)]
42. Yang, Y.; Koo, S.; Lin, C.S.; Neu, B. Macromolecular depletion modulates the binding of red blood cells to activated endothelial cells. *Biointerphases* **2010**, *5*, FA19–FA23. [[CrossRef](#)] [[PubMed](#)]
43. Nieuwdorp, M.; van Haeften, T.W.; Gouverneur, M.C.; Mooij, H.L.; van Lieshout, M.H.; Levi, M.; Meijers, J.C.; Holleman, F.; Hoekstra, J.B.; Vink, H.; et al. Loss of endothelial glycocalyx during acute hyperglycemia coincides with endothelial dysfunction and coagulation activation in vivo. *Diabetes* **2006**, *55*, 480–486. [[CrossRef](#)] [[PubMed](#)]
44. Martinez-Ramirez, S.; Greenberg, S.M.; Viswanathan, A. Cerebral microbleeds: Overview and implications in cognitive impairment. *Alzheimers Res. Ther.* **2014**, *6*, 33. [[CrossRef](#)] [[PubMed](#)]
45. Qiu, C.; Cotch, M.F.; Sigurdsson, S.; Jonsson, P.V.; Jonsdottir, M.K.; Sveinbjrnsdottir, S.; Eiriksdottir, G.; Klein, R.; Harris, T.B.; van Buchem, M.A.; et al. Cerebral microbleeds, retinopathy and dementia: The AGES-Reykjavik study. *Neurology* **2010**, *75*, 2221–2228. [[CrossRef](#)] [[PubMed](#)]
46. Price, T.O.; Eranki, V.; Banks, W.A.; Ercal, N.; Shah, G.N. Topiramate treatment protects blood-brain barrier pericytes from hyperglycemia-induced oxidative damage in diabetic mice. *Endocrinology* **2012**, *153*, 362–372. [[CrossRef](#)] [[PubMed](#)]
47. Johnson, P.C.; Brendel, K.; Meezan, E. Thickened cerebral cortical capillary basement membranes in diabetics. *Arch. Pathol. Lab. Med.* **1982**, *106*, 214–217. [[PubMed](#)]
48. Cherian, S.; Roy, S.; Pinheiro, A.; Roy, S. Tight Glycemic Control Regulates Fibronectin Expression and Basement Membrane Thickening in Retinal and Glomerular Capillaries of Diabetic Rats. *Investig. Ophthalmol. Vis. Sci.* **2009**, *50*, 943–949. [[CrossRef](#)] [[PubMed](#)]
49. Liddelow, S.A.; Guttenplan, K.A.; Clarke, L.E.; Bennett, F.C.; Bohlen, C.J.; Schirmer, L.; Bennett, M.L.; Münch, A.E.; Chung, W.S.; Peterson, T.C.; et al. Neurotoxic reactive astrocytes are induced by activated microglia. *Nature* **2017**, *541*, 481–487. [[CrossRef](#)] [[PubMed](#)]
50. Iliff, J.J.; Wang, M.; Liao, Y.; Plogg, B.A.; Peng, W.; Gundersen, G.A.; Benveniste, H.; Vates, G.E.; Deane, R.; Goldman, S.A.; et al. A Paravascular Pathway Facilitates CSF Flow Through the Brain Parenchyma and the Clearance of Interstitial Solutes, Including Amyloid β . *Sci. Transl. Med.* **2012**, *4*, 147ra111. [[CrossRef](#)] [[PubMed](#)]
51. Iliff, J.J.; Nedergaard, M. Is there a cerebral lymphatic system? *Stroke* **2013**, *44*, S93–S95. [[CrossRef](#)] [[PubMed](#)]
52. Jessen, N.A.; Munk, A.S.; Lundgaard, I.; Nedergaard, M. The glymphatic system—A beginner's guide. *Neurochem. Res.* **2015**, *40*, 2583–2599. [[CrossRef](#)] [[PubMed](#)]
53. Abbott, N.J.; Pizzo, M.E.; Preston, J.E.; Janigro, D.; Thorne, R.G. The role of brain barriers in fluid movement in the CNS: Is there a 'glymphatic' system? *Acta Neuropathol.* **2018**, *135*, 387–407. [[CrossRef](#)] [[PubMed](#)]
54. Weller, R.O.; Sharp, M.M.; Christodoulides, M.; Carare, R.O.; Mollgard, K. The meninges as barriers and facilitators for the movement of fluid, cells and pathogens related to the rodent and human CNS. *Acta Neuropathol.* **2018**, *135*, 363–385. [[CrossRef](#)] [[PubMed](#)]
55. Bacyinski, A.; Maosheng, X.U.; Wang, W.; Hu, J. The paravascular pathway for brain current understanding, significance and controversy. *Front. Neuroanat.* **2017**, *11*, 101. [[CrossRef](#)] [[PubMed](#)]
56. Albargothy, N.J.; Johnston, D.A.; MacGregor-Sharp, M.; Weller, R.O.; Verma, A.; Hawkes, C.A.; Carare, R.O. Convective influx/glymphatic system: Tracers injected into the CSF enter and leave the brain along separate periaxonal basement membrane pathways. *Acta Neuropathol.* **2018**. [[CrossRef](#)] [[PubMed](#)]
57. Nilsson, P.M. Early vascular aging (EVA): Consequences and Prevention. *Vasc. Health Risk Manag.* **2008**, *4*, 547–552. [[CrossRef](#)] [[PubMed](#)]
58. Wrighten, S.A.; Piroli, G.G.; Grillo, C.A.; Reagan, L.P. A look inside the diabetic brain: Contributors to diabetes-induced brain aging. *Biochim. Biophys. Acta* **2009**, *1792*, 444–453. [[CrossRef](#)] [[PubMed](#)]
59. Ryan, C.M.; Geckle, M. Why is learning and memory dysfunction in Type 2 diabetes limited to older adults? *Diabetes Metab. Res. Rev.* **2000**, *16*, 308–315. [[CrossRef](#)]

60. De Pablo-Fernandez, E.; Goldacre, R.; Pakpoor, J.; Noyce, A.J.; Warner, T.T. Association between diabetes and subsequent Parkinson disease: A record-linkage cohort study. *Neurology* **2018**. [[CrossRef](#)] [[PubMed](#)]
61. Knott, G.; Marchman, H.; Wall, D.; Lich, B. Serial section scanning electron microscopy of adult brain tissue using focused ion beam milling. *J. Neurosci.* **2008**, *28*, 2959–2964. [[CrossRef](#)] [[PubMed](#)]
62. Pizzo, M.E.; Wolak, D.J.; Kumar, N.N.; Brunette, E.; Brunquell, C.L.; Hannocks, M.J.; Abbott, N.J.; Meyerand, M.E.; Sorokin, L.; Stanimirovic, D.B.; et al. Intrathecal antibody distribution in the rat brain: Surface diffusion, perivascular transport and osmotic enhancement of delivery. *J. Physiol.* **2018**, *596*, 445–475. [[CrossRef](#)] [[PubMed](#)]



© 2018 by the authors. Licensee MDPI, Basel, Switzerland. This article is an open access article distributed under the terms and conditions of the Creative Commons Attribution (CC BY) license (<http://creativecommons.org/licenses/by/4.0/>).